STABILITY PROPERTIES OF A FIELD-REVERSED ION LAYER IN A BACKGROUND PLASMA

by

Han S. Uhm and Ronald C. Davidson

PFC/JA-78-7

Submitted to Physics of Fluids, August 1978

STABILITY PROPERTIES OF A FIELD-REVERSED ION LAYER IN A BACKGROUND PLASMA

Han S. Uhm* and Ronald C. Davidson
Plasma Fusion Center
Massachusetts Institute of Technology
Cambridge, Massachusetts 02139

ABSTRACT

Stability properties of an intense proton layer (P-layer) immersed in a background plasma are investigated within the framework of a hybrid model in which the layer ions are described by the Vlasov equation, and the background plasma electrons and ions are described as macroscopic, cold fluids. Moreover, the stability analysis is carried out for frequencies near multiples of the mean rotational frequency of the layer. It is assumed that the layer is thin, with radial thickness (2a) much smaller than the mean radius (R_0). Electromagnetic stability properties are calculated for flute perturbations ($\partial/\partial z=0$) about a P-layer with rectangular density profile, described by the rigid-rotor equilibrium distribution function $f_b^0=(m_i n_b/2\pi)\delta(U-\hat{T})G(v_z)$, where n_b and $\hat{T}$ are constants, m_i is the mass of the layer ions, $G(v_z)$ is the parallel velocity distribution, and U is an effective perpendicular energy variable. Stability properties are investigated including the effects of (a) the equilibrium magnetic field depression produced by the P-layer, (b) transverse magnetic perturbations ($\delta\underset{\sim}{B}\neq 0$), (c) small (but finite) transverse temperature of the layer ions, and (d) the dielectric properties of the background plasma. All of these effects are shown to have an important influence on stability behavior. For example, for a dense background plasma, the system can be easily stabilized by a sufficiently large transverse temperature of the layer ions.

*Permanent address: Nuclear Branch, Naval Surface Weapons Center. Silver Spring, Md. 20910

I. INTRODUCTION

Field-reversed ion layers and rings have received considerable recent attention as magnetic confinement configurations for fusion plasmas.[1-8] Such layers and rings are likely subject to various macro- and microinstabilities.[9-13] For example, recent theoretical studies of the negative-mass[11-13] stability properties of a weakly diamagnetic ion layer embedded in a background plasma predict instability[13] for perturbations with frequency near harmonics of the layer rotational frequency. These studies[13] have been carried out for a low-intensity ion layer characterized by $\nu<<1$, where $\nu=N_b e^2/m_i c^2$ is Budker's parameter for the layer ions, and $N_b=2\pi\int_0^{R_c} dr\, r\, n_b^0(r)$ is the number of ions per unit axial length. A more general stability analysis is required to investigate stability properties for an intense field-reversed ion layer characterized by $\nu>>1$.

This paper develops a hybrid theory of the negative-mass instability for intense ion layers with arbitrary degree of field reversal. The present work extends the previous self-consistent theory[13] of the negative-mass instability developed for $\nu<<1$. The analysis is carried out within the framework of a hybrid (Vlasov-fluid) model in which the layer electrons and background plasma electrons and ions are described as macroscopic, cold fluids immersed in an axial magnetic field $B_z^0(r)\hat{e}_z$, and the layer ions are described by the Vlasov equation. We assume that the layer is thin [Eq. (1)], i.e., the radial thickness (2a) of the layer is small in comparison with the mean radius R_0. Equilibrium and stability properties are calculated for the specific choice of ion layer distribution function [Eq. (2)]

$$f_b^0(H_\perp-\omega_\theta P_\theta,\ v_z) = \frac{m_i n_b}{2\pi}\,\delta(U-\hat{T})G(v_z)\ ,$$

where n_b, ω_θ, $\hat{T}$ are constants, $G(v_z)$ is the parallel velocity distribution, $H_\perp$ is the perpendicular energy, P_θ is the canonical angular momentum, and U is the effective energy variable defined in Eq. (3).

One of the important features of the equilibrium analysis (Sec. II) is that the equilibrium distribution function in Eq. (2) corresponds to a sharp-boundary density profile [Eq. (9)], with uniform angular velocity profile over the layer cross section [Eq. (12)], and nonzero transverse temperature [Eq. (13)]. Moreover, defining the magnetic compression ratio η by $\eta=B_z^0(r=R_1)/B_0$ [Eq. (16)], where $B_z^0(r=R_1)$ and B_0 are the axial magnetic fields at the inner and outer surfaces of the layer, we find [Eq. (26)]

$$\nu=(1-\eta)/(1+\eta) ,$$

for a thin layer with $a<<R_0$. Because $\nu\geq 0$, it is important to note from Eq. (26) that the allowable range of compression ratio is given by $-1<\eta\leq 1$. Moreover, in order to produce a sizeable field depression, a relatively large value of Budker's parameter ($\nu\gtrsim 1$) is required. We also emphasize that the rigid-rotor distribution function in Eq. (2) has an associated spread in canonical angular momentum (Δ) [Eq. (32)], which plays an important role in determining stability behavior.[11]

The electromagnetic stability analysis in Secs. III-V includes the effects of (a) the equilibrium magnetic field depression produced by the P-layer, (b) transverse magnetic perturbations ($\delta\underset{\sim}{B}\neq 0$), (c) small (but finite) transverse temperature of the layer ions, and (d) the dielectric properties of the background plasma. The analysis is carried out within the framework of the linearized Vlasov-fluid and Maxwell equations, assuming that all perturbed quantities are independent of

axial coordinate ($\partial/\partial z=0$). Moreover, the stability properties are investigated for eigenfrequency near multiples of the mean P-layer rotational frequency, i.e., $|\omega-\ell\omega_\theta| \ll \omega_r$, where ω is the complex eigenfrequency, ℓ is the azimuthal harmonic number, ω_θ is the mean rotational frequency of the P-layer, and ω_r is the radial betatron frequency of the layer ions. It is also assumed that the background plasma has a step-function density profile (Fig. 5).

The formal stability analysis for perturbations with $\partial/\partial z=0$ is carried out in Secs. III and IV. The perturbed charge density of the layer ions is calculated in Sec. III, including kinetic ion orbit effects. A fully electromagnetic eigenvalue equation is obtained in Sec. IV, including the dielectric properties of the background plasma. Equation (69), when combined with Eq. (68), constitute one of the main results of this paper and can be used to investigate stability properties for a broad range of system parameters. In this regard, we emphasize that Eq. (69) has been derived with no a priori restriction on the background plasma density.

In Sec. V, a detailed analytic investigation of electromagnetic stability properties is carried out for a dense plasma background. For certain ranges of system parameters, it is found that the system is unstable. Moreover, the instability mechanism is similar to that for the negative-mass instability,[11-13] including the effects of transverse temperature of the layer ions, and the dielectric properties of the background plasma. For example, in the case where the plasma density outside the layer is equal to zero ($\alpha=0$), the approximate dispersion relation is given by [Eq. (90)]

$$\frac{\zeta'}{\zeta}\,\Omega^3 + \Omega^2 - \ell\lambda\,\frac{\zeta'}{\zeta}\,\Omega + 2\lambda\left(\frac{2\eta}{\zeta(1+\eta)} - \frac{\ell}{2}\right) = 0 \ ,$$

where Ω is the normalized Doppler-shifted eigenfrequency defined in Eq. (88), and the parameters ζ and λ are defined in Eqs. (87) and (91), respectively. In Eq. (90), ζ' [Eq. (87)] is an oscillatory function of plasma density. However, the value of ζ', averaged over each period, is an increasing function of plasma density. We therefore conclude from Eq. (90) that the system is completely stabilized if the plasma density is sufficiently high. The terms proportional to $\ell\lambda$ in Eq. (90) also have a stabilizing influence, thereby quenching the growth rate for sufficiently high ℓ values. This effect is most pronounced when the magnetic compression ratio η is close to zero. A similar stabilization for high ℓ values has also been demonstrated for intense relativistic E-layers.[11]

A numerical investigation of stability properties is carried out in Sec. V.C for general values of αn_p (the plasma density outside the layer). Several points are noteworthy in this regard. First, the instability growth rate is greatly reduced as $\eta \to 0$. This feature is evident from Eq. (90) for $\alpha=0$. Second, stability properties are almost independent of α, provided α is sufficiently small ($\alpha \lesssim 0.5$, say). Finally, in parameter regimes where instability does exist, the maximum growth rate can be a substantial fraction of ion cyclotron frequency $\hat{\omega}_{ci}$.

In Sec. VI, a numerical investigation of stability properties is carried out for an arbitrary value of background plasma density, assuming a rectangular density profile with $\alpha = 0$. The eigenfunction $\hat{\phi}(r)$ is obtained numerically from the eigenvalue equation (72). It is found from the numerical analysis that the electrostatic eigenfunction $\hat{\phi}(r)=(r/R_0)^{\ell}$

is a very good approximation to the actual eigenfunction for a field-reversed ion layer in a low-density background plasma satisfying $\hat{\omega}_{pi}R_0/c < 1$, where $\hat{\omega}_{pi}$ is the background ion plasma frequency and c is the speed of light in vacuo. However, the electromagnetic effects associated with the background plasma dielectric response become dominant when the plasma density is sufficiently high that $\hat{\omega}_{pi}R_0/c \gtrsim 2$. Generally speaking, the numerical investigation of stability properties in Sec. VI gives similar results to those obtained analytically in Sec. V.

II. EQUILIBRIUM THEORY

A. General Equilibrium Properties

The equilibrium configuration is illustrated in Fig. 1. It consists of a space-charge neutralized P-layer (proton layer) that is infinite in axial extent and immersed in a cold, dense, background plasma. The plasma ions are assumed to be singly charged, and the mean radius and radial thickness of the P-layer are denoted by R_0 and 2a, respectively. The radius of the cylindrical conducting wall is denoted by R_c. The mean motion of the P-layer is in the azimuthal direction, and the applied and self magnetic field provides radial confinement of the layer ions. As shown in Fig. 1, we introduce a cylindrical polar coordinate system (r,θ,z) with z-axis coinciding with the axis of symmetry; r is the radial distance from the z-axis, and θ is the polar angle in a plane perpendicular to the z-axis. The following are the main assumptions pertaining to the equilibrium configuration:

(a) Equilibrium properties are azimuthally symmetric ($\partial/\partial\theta=0$) and independent of z.

(b) The radial thickness of the P-layer is much smaller than its major radius, i.e.,

$$a \ll R_0 \ . \tag{1}$$

(c) The background plasma electrons (j=e) and ions (j=i), and the layer electrons (j=e') are treated as macroscopic cold fluids ($T_j=0$). In equilibrium, these fluids are assumed to be stationary with zero net axial motion [$V^0_{zj}(r)=0$] and zero net azimuthal motion [$V^0_{\theta j}(r)=\omega_j(r)r=0$] for j=e,i,e'.

(d) The background plasma equilibrium is assumed to be electrically neutral with $n_i^0(r)=n_e^0(r)$. In addition, the equilibrium charge density of the layer ions (j=b) is neutralized by the layer electrons (j=e') with $n_b^0(r)=n_{e'}^0(r)$, and the equilibrium radial electric field is equal to zero, $E_r^0(r)=0$.

For the layer ions, any distribution function $f_b^0(\mathcal{E},\mathcal{P})$ that is a function of the single-particle constants of the motion in the equilibrium fields is a solution to the steady-state ($\partial/\partial t=0$) Vlasov equation. For present purposes, we consider the class of rigid-rotor Vlasov equilibria described by[4]

$$f_b^0(H_\perp-\omega_\theta P_\theta,\ v_z) = \frac{m_i n_b}{2\pi}\,\delta(U-\hat{T})G(v_z)\ , \tag{2}$$

where n_b, ω_θ, and $\hat{T}$ are constants, $G(v_z)$ is the parallel velocity distribution with normalization $\int_{-\infty}^{\infty} dv_z G(v_z)=1$, and the effective energy variable U is defined by

$$U=H_\perp-\omega_\theta P_\theta+m_i R_0^2\omega_\theta^2/2+(e/c)R_0\omega_\theta A_\theta^0(R_0)\ . \tag{3}$$

In Eq. (3), $H_\perp$ is the perpendicular energy

$$H_\perp=(m_i/2)(v_r^2+v_\theta^2)\ , \tag{4}$$

and P_θ is the canonical angular momentum

$$P_\theta=r[m_i v_\theta+(e/c)A_\theta^0(r)]\ . \tag{5}$$

Here e and m_i are the proton charge and mass, respectively, c is the speed of light in vacuo, and v_r and v_θ are the radial and axial velocities of a layer ion. The θ-component of the equilibrium vector potential, $A_\theta^0(r)$, is to be calculated self-consistently from the steady-state

Maxwell equation,

$$\frac{\partial}{\partial r}\frac{1}{r}\frac{\partial}{\partial r}\, rA_\theta^0(r) = -\frac{4\pi e}{c}\, n_b^0(r) V_\theta^0(r) \ , \tag{6}$$

where $n_b^0(r)$ is the local ion layer density,

$$n_b^0(r)=\int d^3v\ f_b^0(H_\perp-\omega_\theta P_\theta,\ v_z) \ , \tag{7}$$

and $V_\theta^0(r)$ is the mean azimuthal velocity of an ion layer fluid element,

$$V_\theta^0(r)=\left(\int d^3v\ v_\theta f_b^0\right)/\left(\int d^3v\ f_b^0\right) \ . \tag{8}$$

Substituting Eq. (2) into Eq. (7), we find that the ion layer density is given by (Fig. 2)

$$n_b^0(r) = \begin{cases} n_b \ , & R_1<r<R_2 \ , \\ 0 \ , & \text{otherwise} \ , \end{cases} \tag{9}$$

where R_1 and R_2 are the extremes of the interval on which the inequality

$$\psi(r)\geq 0 \tag{10}$$

is satisfied. [That is, R_1 and R_2 are determined from $\psi(R_1)=\psi(R_2)=0$.] In Eq. (10), the envelope function $\psi(r)$ is defined by

$$\psi(r)=(m_i\omega_\theta^2/2)(r^2-R_0^2)+(e/c)\omega_\theta[rA_\theta^0(r)-R_0A_\theta^0(R_0)]+\hat{T} \ . \tag{11}$$

From Eqs. (2) and (11), $\psi(r)=(m_i/2)[v_r^2+(v_\theta-r\omega_\theta)^2]$ is the $(r-\theta)$ kinetic energy of a layer ion in a frame of reference rotating with angular velocity ω_θ. In a similar manner, the azimuthal velocity profile associated with the equilibrium distribution function in Eq. (2) can be expressed as

$$v_\theta^0(r)=r\omega_\theta \ , \quad R_1<r<R_2 \ . \tag{12}$$

Equation (12) corresponds to a rigid-rotor angular velocity profile over the layer cross section. Defining the effective temperature $T_\perp^0(r)$ for the transverse motion of the layer ions by

$$n_b^0(r)T_\perp^0(r)=\frac{m_i}{2}\int d^3v[v_r^2+(v_\theta-r\omega_\theta)^2]f_b^0 \ ,$$

we find from Eqs. (2) and (11) that the transverse temperature profile can be expressed as

$$T_\perp^0(r)=\psi(r) \ , \quad R_1<r<R_2 \ . \tag{13}$$

Evidently, the envelope function $\psi(r)\geq 0$ defined in Eq. (11) is identical to the transverse temperature profile.

We note from Eq. (9) that the density profile has sharp radial boundaries at R_1 and R_2. Substituting Eq. (12) into Eq. (6), we find that the equilibrium axial magnetic field within the P-layer $(R_1<r<R_2)$ can be expressed as

$$B_z^0(r)=B_0+(2\pi e/c)\omega_\theta n_b(R_2^2-r^2) \ , \tag{14}$$

where B_0 is the axial magnetic field at $r\geq R_2$. The corresponding equilibrium vector potential $A_\theta^0(r)$ is given by

$$rA_\theta^0(r)=R_0A_\theta^0(R_0)+(B_0/2)(r^2-R_0^2)$$
$$+(\pi e/2c)\omega_\theta n_b(r^2-R_0^2)[2R_2^2-(r^2+R_0^2)] \ . \tag{15}$$

For notational convenience in the subsequent analysis, we introduce the magnetic compression ratio η defined by

$$\eta=B_z^0(r=R_1)/B_0 \ , \tag{16}$$

which characterizes the change in axial magnetic field. We further introduce Budker's parameter for the layer ions

$$\nu=2\pi(e^2/m_ic^2)\int_0^{R_c} dr\ r\ n_b^0(r) \ . \tag{17}$$

Substituting Eq. (14) into Eq. (16) and making use of Eq. (17) gives

$$\omega_\theta/\hat{\omega}_{ci}=(\eta-1)/2\nu \ , \tag{18}$$

where $\hat{\omega}_{ci}=eB_0/m_ic$ is the ion cyclotron frequency at $r=R_2$. The axial magnetic field profile is illustrated in Fig. 3.

Equations (11) and (15) completely determine the functional form of the envelope function $\psi(r)$. We note from Eq. (15) that equilibrium layer density (the term proportional to n_b) can generally have a large nonlinear influence on the location of the radial boundaries R_1 and R_2. A sketch of $\psi(r)$ versus r is illustrated in Fig. 4. Thus far, R_0 has been introduced in the analysis as an unspecified constant parameter in Eq. (3). Without loss of generality, we choose R_0 to correspond to that radius where $\psi(r)$ passes through a maximum in the interval $R_1<r<R_2$ (Fig. 4),

$$\left(\frac{\partial}{\partial r}\ \psi(r)\right)_{r=R_0}=0 \ . \tag{19}$$

Substituting Eq. (11) into Eq. (19) we find

$$\omega_\theta+(e/m_ic)B_z^0(R_0)=0 \ , \tag{20}$$

where use has been made of Eqs. (14) and (15).

Equation (20) is simply a statement of radial force balance on an ion layer fluid element at $r=R_0$. Further general equilibrium properties associated with the distribution function in Eq. (2) are discussed in Ref. 4.

B. Thin-Layer Approximation with $a/R_0<<1$

We now specialize to the case of a thin layer with $(R_2-R_1)/R_0<<1$, and Taylor-expand Eq. (11) about $r=R_0$,

$$\psi(r)=\hat{T} - \frac{1}{2} m_i\omega_r^2(r-R_0)^2 + \ldots \tag{21}$$

where

$$\omega_r^2 = - \frac{1}{m_i}\left(\frac{\partial^2\psi}{\partial r^2}\right)_{r=R_0} = - \frac{e\omega_\theta}{m_i c} R_0 \left(\frac{\partial}{\partial r} B_z^0(r)\right)_{r=R_0} = \omega_b^2\beta_0^2 \tag{22}$$

Here, ω_r can be identified with the betatron frequency for radial oscillations about the equilibrium radius R_0. In Eq. (22), $\omega_b^2=4\pi e^2 n_b/m_i$ is the plasma frequency-squared for the layer ions, and $\beta_0^2=R_0^2\omega_\theta^2/c^2$. Defining the half-thickness of the layer by

$$a=(2\hat{T}/m_i)^{1/2}/\omega_r \ , \tag{23}$$

we readily determine $R_1=R_0-a$ and $R_2=R_0+a$ from $\psi(r)=0$ and Eq. (21). It is also noteworthy from Eq. (22) that the betatron frequency ω_r is directly proportional to $\omega_b\beta_0$ for the rigid-rotor equilibrium described by Eq. (2). This is considerably different from the result obtained in Ref. 12 for the choice of distribution function in which all of the layer ions have the same values of canonical angular momentum and the same value of energy.

For a thin P-layer, it is straightforward to show

$$\left(\frac{\partial}{\partial r}\psi(r)\right)_{r=R_1} = - \left(\frac{\partial}{\partial r}\psi(r)\right)_{r=R_2} \tag{24}$$

from Eq. (21). Substituting Eq. (11) into Eq. (24) and making use of definition in Eq. (16) gives

$$\omega_\theta/\hat{\omega}_{ci}=-(1+\eta)/2 \ , \tag{25}$$

which determines the rotational frequency ω_θ in terms of the compression ratio η. Moreover, substituting Eq. (25) into Eq. (18), we find

$$\nu=(1-\eta)/(1+\eta) \ . \tag{26}$$

Equation (26) is one of the most important equilibrium results pertaining to the choice of distribution function in Eq. (2), and several points are noteworthy. First, Budker's parameter ν for the layer ions can be expressed exclusively in terms of the magnetic field compression ratio η. Second, since $\nu \geq 0$, the allowed range of η is given by

$$-1<\eta\leq 1 \ . \tag{27}$$

Moreover, Budker's parameter rapidly increases to infinity as the compression ratio approaches minus unity ($\eta \to -1$). In this regard, strictly speaking, it is not possible to achieve complete field reversal ($\eta \equiv -1$) for the choice of distribution function in Eq. (2). We note that $\nu=1$ corresponds to zero compression ratio ($\eta=0$). Therefore, in order to produce a significant field depression, we conclude that a layer with a reasonably high value of Budker's parameter ($\nu \gtrsim 1$) is necessary.

Of considerable interest for experimental application is the relationship between the applied axial magnetic field $\hat{B}$ before injection of the layer, and the external magnetic field B_0 after injection. In this regard, we assume that the magnetic flux inside the cylindrical

conductor is conserved, i.e.,

$$2\pi\int_0^{R_c} rdr\ B_z^0(r)=\pi R_c^2\hat{B}\ . \tag{28}$$

For a thin layer, the axial magnetic field profile can be approximated by

$$B_z^0(r) = B_0\begin{cases}\eta\ , & 0<r<R_0\ ,\\ 1\ , & R_0<r<R_c\ ,\end{cases}$$

and it is straightforward to show from Eq. (28) that

$$\hat{B}/B_0=1-(1-\eta)(R_0/R_c)^2\ . \tag{29}$$

For $\hat{B}/B_0>0$, we conclude from Eq. (29) that the magnetic compression ratio is restricted to

$$-\eta<(R_c/R_0)^2-1\ . \tag{30}$$

Finally, we conclude this section by noting that the choice of equilibrium distribution function in Eq. (2) yields a spread in canonical angular momentum P_θ. Defining the average canonical angular momentum P_0 as

$$P_0=m_iR_0^2\omega_\theta+(e/c)R_0A_\theta^0(R_0)\ ,$$

it is straightforward to show from Eqs. (2) and (11) that

$$|P_\theta-P_0|=m_iR_0[2\hat{T}/m_i-v_r(R_0)^2]^{1/2}, \tag{31}$$

where $v_r(R_0)$ is the radial velocity of a layer ion at $r=R_0$. For a given transverse temperature $\hat{T}$, those particles with $v_r(R_0)=0$ have the maximum deviation in canonical angular momentum from the mean value P_0. Therefore, the maximum canonical angular momentum spread Δ can be

expressed as

$$\Delta = |P_\theta - P_0|_m = R_0(2m_i\hat{T})^{1/2} . \tag{32}$$

The parameter Δ defined in Eq. (32) plays an important role in determining the stability properties[10] discussed in Secs. III and IV.

III. PERTURBED CHARGE DENSITY FOR A THIN ION LAYER

In the present article, we consider perturbations with very long axial wavelength ($k_z^2 R_0^2 << 1$), and approximate

$$k_z = 0 \tag{33}$$

in the subsequent analysis. (Here k_z is the axial wavenumber.) It is assumed that all perturbed quantities $\delta\psi(\underset{\sim}{x},t)$ can be Fourier-decomposed according to

$$\delta\psi(\underset{\sim}{x},t) = \hat{\psi}_\ell(r)\exp\{i(\ell\theta-\omega t)\}, \quad \mathrm{Im}\omega > 0 \ , \tag{34}$$

where ω is the complex eigenfrequency, and ℓ is the azimuthal harmonic number. Moreover, the stability analysis is carried out for eigenfrequency near multiples of the mean P-layer rotational frequency, i.e., $\omega \simeq \ell\omega_\theta$.

The Maxwell equations for the perturbed fields become

$$\underset{\sim}{\nabla}\times\hat{\underset{\sim}{E}}(\underset{\sim}{x}) = i(\omega/c)\hat{\underset{\sim}{B}}(\underset{\sim}{x}) \ ,$$
$$\underset{\sim}{\nabla}\times\hat{\underset{\sim}{B}}(\underset{\sim}{x}) = (4\pi/c)\hat{\underset{\sim}{J}}(\underset{\sim}{x}) - i(\omega/c)\hat{\underset{\sim}{E}}(\underset{\sim}{x}) \ .$$

Within the context of Eq. (33), the perturbed electromagnetic fields can be expressed as

$$\hat{\underset{\sim}{E}}_\ell(r) = \hat{E}_{\ell r}(r)\hat{\underset{\sim}{e}}_r + \hat{E}_{\ell\theta}(r)\hat{\underset{\sim}{e}}_\theta \ ,$$
$$\hat{\underset{\sim}{B}}_\ell(r) = \hat{B}_{\ell z}(r)\hat{\underset{\sim}{e}}_z \ . \tag{35}$$

Fourier decomposing the perturbed fields according to Eqs. (34) and (35), the $\underset{\sim}{\nabla}\times\hat{\underset{\sim}{B}}$ and $\underset{\sim}{\nabla}\times\hat{\underset{\sim}{E}}$ Maxwell equations can be expressed as

$$\hat{E}_{\ell r}(r)=\ell^2(\omega^2r^2/c^2-\ell^2)^{-1}(\partial/\partial r)\hat{\phi}$$
$$-4\pi ir^2\omega(\omega^2r^2-\ell^2c^2)^{-1}\hat{J}_{\ell r}(r) \ ,$$
$$\hat{B}_{\ell z}(r)=-\ell\omega r(\omega^2r^2/c-\ell^2c)^{-1}(\partial/\partial r)\hat{\phi} \tag{36}$$
$$+4\pi ir\ell(\omega^2r^2/c-\ell^2c)^{-1}\hat{J}_{\ell r}(r) \ ,$$

where the function $\hat{\phi}(r)$ is defined by

$$\hat{\phi}(r)=ir\hat{E}_{\ell\theta}(r)/\ell \ , \tag{37}$$

and $\hat{J}_{\ell r}(r)$ is the perturbed radial current density.

After some straightforward algebra, the perturbed ion layer distribution function can be expressed as[11]

$$\hat{f}_{b\ell}(r,\underset{\sim}{y})=e\frac{\partial f_b^0}{\partial U}\int_{-\infty}^{0}d\tau\ \exp\{-i[\omega\tau-\ell(\theta'-\theta)]\}$$
$$\times\left[(\dot{\theta}'-\omega_\theta)\left(i\ell\hat{\phi}+\frac{r'v_r'}{c}\hat{B}_{\ell z}\right)-\left(\hat{E}_{\ell r}+\frac{v_\theta'}{c}\hat{B}_{\ell z}\right)v_r'\right] \ , \tag{38}$$

where $\tau=t'-t$. In obtaining Eq. (38), use has been made of $\partial U/\partial\underset{\sim}{y}=m_i[v_r\hat{\underset{\sim}{e}}_r+(v_\theta-r\omega_\theta)\hat{\underset{\sim}{e}}_\theta]$, where $\hat{\underset{\sim}{e}}_r$ and $\hat{\underset{\sim}{e}}_\theta$ are unit vectors in the r and θ directions, respectively. In Eq. (38), the trajectories, $\underset{\sim}{x}'(t')$ and $\underset{\sim}{y}'(t')$ satisfy

$$\frac{d}{dt'}\underset{\sim}{x}'=\underset{\sim}{y}' \ , \quad \frac{d}{dt'}\underset{\sim}{y}'=\frac{e}{m_ic}\underset{\sim}{y}'\times\underset{\sim}{B}_0(\underset{\sim}{x}') \ ,$$

where $\underset{\sim}{x}'(t'=t)=\underset{\sim}{x}$, and $\underset{\sim}{y}'(t'=t)=\underset{\sim}{y}$. The term $\hat{E}_{\ell r}+v_\theta\hat{B}_{\ell z}/c$ in Eq. (38) can be further simplified. Making use of Eq. (36) we obtain

$$\hat{E}_{\ell r}(r)+\frac{\omega r}{\ell c}\hat{B}_{\ell z}(r)=-\frac{\partial}{\partial r}\hat{\phi} \ . \tag{39}$$

Since the eigenfrequency of the perturbation is given approximately by $\omega\simeq\ell\omega_\theta$, Eq. (39) can be approximated by

$$\hat{E}_{\ell r}(r)+v_\theta \hat{B}_{\ell z}(r)/c=-(\partial/\partial r)\hat{\phi}(r) \ . \tag{40}$$

The evaluation of the orbit integral in Eq. (38) is generally very complicated. However, for present purposes, we assume low-frequency, long-wavelength perturbations characterized by

$$\begin{aligned} &|\omega-\ell\omega_\theta|^2 << \omega_r^2 \ , \\ &\ell a/R_0 << \omega_r/|\omega_\theta| \ , \end{aligned} \tag{41}$$

where a is the half-thickness of the layer defined in Eq. (23). Within the context of Eq. (41), it is valid for a thin layer to approximate

$$\begin{aligned} &\hat{\phi}(r')=\hat{\phi}(R_0) \ , \\ &\theta'=\theta+[\omega_\theta+(v_\perp/R_0)\cos\alpha]\tau \ , \end{aligned} \tag{42}$$

where $v_\perp$ is the perpendicular speed in a frame of reference rotating with angular velocity ω_θ. Moreover, $v_\perp$ is related to the effective energy variable U by

$$U=(m_i/2)[v_\perp^2+\omega_r^2(r-R_0)^2] \ , \tag{43}$$

with $v_\theta-r\omega_\theta=v_\perp\cos\alpha$ [see Eqs. (3), (11), and (21)]. Furthermore, the perturbed ion layer distribution function can be simplified as [see Appendix A],

$$\hat{f}_{b\ell}(r,\underset{\sim}{v})=i\ell\,\frac{ev_\perp}{R_0}\cos\alpha\,\frac{\partial f_b^0}{\partial U}\int_{-\infty}^{0} d\tau\hat{\phi}\exp\{-i[\omega\tau-\ell(\theta'-\theta)]\} \ . \tag{44}$$

Substituting Eq. (42) into Eq. (44) gives

$$\hat{f}_{b\ell}(r,\underset{\sim}{v})=-e\,\frac{\partial f_b^0}{\partial U}\,\hat{\phi}(R_0)\,\frac{\ell(v_\perp/R_0)\cos\alpha}{(\omega-\ell\omega_\theta)-(\ell v_\perp/R_0)\cos\alpha} \ . \tag{45}$$

The perturbed surface charge density $\sigma_{b\ell}$ for a very thin ion layer ($a<<R_0$) is defined by

$$\sigma_{b\ell} = \frac{e}{2}\int_{R_1}^{R_2} dr \int_0^{2\pi} d\alpha \int_0^{\infty} dv_\perp^2 \int_{-\infty}^{\infty} dv_z \hat{f}_{b\ell}(r,\underset{\sim}{v}) \ . \tag{46}$$

Substituting Eq. (45) into Eq. (46), and making use of $\nu \simeq 4\pi e^2 n_b R_0 a/m_i c$, it is straightforward to show that

$$\sigma_{b\ell} = \frac{1}{2\pi} \frac{\nu \ell^2 c^2 \hat{\phi}(R_0)/R_0^3}{(\omega-\ell\omega_\theta)^2 - \ell^2 \omega_r^2 (a/R_0)^2} \ , \tag{47}$$

where use has been made of Eq. (23). Equation (47) is valid for perturbations about a very thin layer ($a<<R_0$).

IV. ELECTROMAGNETIC STABILITY PROPERTIES

A. General Eigenvalue Equation

As discussed at the beginning of Sec. II, the background plasma components (j=e,i) and layer electrons (j=e') are treated as cold ($T_j \to 0$), macroscopic fluids immersed in an axial magnetic field $B_z^0(r)\hat{e}_z$, where $B_z^0(r)$ is approximated by

$$B_z^0(r)=B_0 \begin{cases} n\ , & 0<r<R_0\ , \\ 1\ , & R_0<r<R_c\ , \end{cases} \tag{48}$$

for a thin layer. The momentum transfer equation and the continuity equation for each cold-fluid component can be expressed as

$$\left(\frac{\partial}{\partial t} + \underset{\sim}{V}_j\cdot\underset{\sim}{\nabla}\right)\underset{\sim}{V}_j = \frac{e_j}{m_j}\left(\underset{\sim}{E} + \frac{\underset{\sim}{V}_j\times\underset{\sim}{B}}{c}\right)\ ,$$

$$(\partial/\partial t)n_j+\underset{\sim}{\nabla}\cdot(n_j\underset{\sim}{V}_j)=0\ , \tag{49}$$

where $n_j(\underset{\sim}{x},t)$ is the density, $\underset{\sim}{V}_j(\underset{\sim}{x},t)$ is the mean velocity, and e_j and m_j are charge and mass, respectively, of a particle of species j.

As illustrated in Fig. 5, the stability properties of the layer-plasma system are investigated for perturbations about the step-function plasma density profiles specified by

$$n_j^0(r)=n_p \begin{cases} 1\ , & 0<r<R_0\ , \\ \alpha\ , & R_0<r<R_c\ , \end{cases} \tag{50}$$

for j=e,i. Here α is an arbitrary constant. To make the stability analysis tractable, the following simplifying assumptions are also made:

(a) The P-layer is immersed in a dense plasma background, i.e.,

$$n_{b\sim} \lesssim n_p \ , \tag{51}$$

which is easily attainable in the parameter regimes of experimental interest.

(b) The perturbed charge density of the layer ions can be represented by the surface charge contribution given in Eq. (47), which is valid for a sufficiently thin layer ($a \ll R_0$) and dense background plasma ($n_{b\sim} \lesssim n_p$).

(c) The influence of current and charge perturbations associated with the layer electrons are neglected in the stability analysis. Although this is a good approximation for an infinitesimally thin layer with $a/R_0 \to 0$, we expect some modifications to the stability behavior associated with finite layer thickness.

For perturbation with $k_z=0$, Eq. (49) can be linearized to give

$$\begin{aligned}
&-i\omega\hat{n}_j(r) + \frac{1}{r}\frac{\partial}{\partial r}[rn_j^0(r)\hat{V}_{jr}(r)] = -i\frac{\ell}{r}n_j^0(r)\hat{V}_{j\theta}(r) \ , \\
&-i\omega\hat{V}_{jr}(r) - \varepsilon_j\omega_{cj}(r)\hat{V}_{j\theta}(r) = \frac{e_j}{m_j}\hat{E}_r(r) \ , \\
&-i\omega\hat{V}_{j\theta}(r) + \varepsilon_j\omega_{cj}(r)\hat{V}_{jr}(r) = -i\frac{e_j}{m_j}\frac{\ell}{r}\hat{\phi}(r) \ ,
\end{aligned} \tag{52}$$

where ℓ is the azimuthal harmonic number, j=e,i denotes plasma species, and use has been made of $V_{zj}^0(r)=V_{\theta j}^0(r)=0$ for j=e,i. In Eq. (52), $\varepsilon_j=\text{sgn } e_j$,

$$\omega_{cj}(r)=\hat{\omega}_{cj}(=eB_0/m_jc)\times\begin{cases} \eta \ , & 0<r<R_0 \ , \\ 1 \ , & R_0<r<R_c \ , \end{cases} \tag{53}$$

is the cyclotron frequency, $\hat{V}_{j\sim}(r)$ and $\hat{n}_j(r)$ are the perturbed fluid

velocity and density, and the abbreviated notation $\hat{\psi}(r)=\hat{\psi}_{\ell}(r)$ has been introduced for the perturbation amplitudes. The perturbed radial electric field $\hat{E}_r(r)$ in Eq. (36) is calculated self-consistently from Eq. (52) and the definition of radial current density

$$\hat{J}_r(r)=\sum_{j=e,i} e_j n_j^0(r)\hat{V}_{jr}(r) \ .$$

Defining

$$\xi=\left[1-(\omega r/\ell c)^2\right]^{-1} \ , \tag{54}$$

we obtain

$$\left[1+\xi\left(\frac{\omega r}{\ell c}\right)^2\sum_j \frac{\omega_{pj}^2(r)}{\nu_j^2}\right]\hat{E}_r(r)$$

$$=-\xi\frac{\partial\hat{\phi}}{\partial r}-\xi\left(\frac{\omega r}{\ell c}\right)^2\sum_j\frac{\omega_{pj}^2(r)}{\nu_j^2}\frac{\varepsilon_j\omega_{cj}(r)}{\omega}\frac{\ell}{r}\hat{\phi} \ , \tag{55}$$

where $\nu_j^2=\omega^2-\omega_{cj}^2(r)$ and $\omega_{pj}^2(r)$ is the plasma frequency-squared defined by

$$\omega_{pj}^2(r)=\hat{\omega}_{pj}^2(=4\pi e^2 n_p/m_j)\times\begin{cases}1 \ , & 0<r<R_0 \ ,\\ \alpha \ , & R_0<r<R_c \ .\end{cases} \tag{56}$$

Poisson's equation for the perturbed electric field can be expressed as

$$\frac{1}{r}\frac{\partial}{\partial r}\left[r\hat{E}_r(r)\right]+\frac{\ell^2}{r^2}\hat{\phi}(r)=4\pi\sigma_b\delta(r-R_0)+4\pi\sum_j e_j\hat{n}_j(r) \ , \tag{57}$$

where the surface charge density σ_b is defined in Eq. (47). Eliminating $\hat{V}_{jr}(r)$ and $\hat{V}_{j\theta}(r)$ from Eq. (52) in favor of $\hat{n}_j(r)$, and substituting $\hat{n}_j(r)$ into Eq. (57) gives

$$\frac{1}{r}\frac{\partial}{\partial r}\left\{r\left[1-\sum_j\frac{\omega_{pj}^2(r)}{\nu_j^2}\right]\hat{E}_r(r)\right\}+\frac{\ell^2}{r^2}\left[1-\sum_j\frac{\omega_{pj}^2(r)}{\nu_j^2}\right]\hat{\phi}(r)$$

$$=\frac{\ell}{r}\hat{\phi}(r)\sum_j\frac{1}{\omega}\frac{\partial}{\partial r}\left\{\frac{\omega_{pj}^2(r)}{\nu_j^2}\left[\varepsilon_j\omega_{cj}(r)\right]\right\}$$

$$+\frac{\ell}{r}\left(\frac{\partial\hat{\phi}}{\partial r}+\hat{E}_r(r)\right)\sum_j\frac{1}{\omega}\left\{\frac{\omega_{pj}^2(r)}{\nu_j^2}\left[\varepsilon_j\omega_{cj}(r)\right]\right\}$$

$$+\frac{2\ell^2c^2\nu\hat{\phi}/R_0^3}{(\omega-\ell\omega_\theta)^2-\ell^2\omega_r^2(a/R_0)^2}\,\delta(r-R_0)\ , \tag{58}$$

where $\nu=4\pi e^2n_bR_0a/m_ic$ is Budker's parameter for the layer ions. It is useful to introduce the abbreviated notation

$$S_1(r,\omega)=\sum_j\frac{\omega_{pj}^2(r)}{\nu_j^2}-1\ ,$$

$$S_2(r,\omega)=\sum_j\frac{\omega_{pj}^2(r)}{\nu_j^2}\,\frac{\varepsilon_j\omega_{cj}(r)}{\omega}\ , \tag{59}$$

$$S_3(r,\omega)=1+\xi\left(\frac{\omega r}{\ell c}\right)^2\sum_j\frac{\omega_{pj}^2(r)}{\nu_j^2}\ .$$

Eliminating $\hat{E}_r(r)$ from Eqs. (55) and (58), and making use of the definitions in Eq. (59) gives the eigenvalue equation

$$\frac{1}{r}\frac{\partial}{\partial r}\left(\xi\,\frac{S_1}{S_3}\,r\,\frac{\partial\hat{\phi}}{\partial r}\right)$$

$$-\frac{\ell^2}{r^2}\,\frac{S_1}{S_3}\left[1-\xi\left(\frac{\omega r}{\ell c}\right)^2\left(\frac{S_2^2}{S_1}-S_1+1\right)\right]\hat{\phi}$$

$$=\frac{\ell}{r}\,\hat{\phi}\,\frac{\partial}{\partial r}\left\{\frac{S_2}{S_3}\left[1+\xi\left(\frac{\omega r}{\ell c}\right)^2\right]\right\}+4\pi\sigma_b\delta(r-R_0)\ , \tag{60}$$

where σ_b is defined in Eq. (47).

The eigenvalue equation (60) is fully electromagnetic and has been derived with no a priori assumption on the relative strengths of the transverse magnetic and electric perturbations. If we formally take the electrostatic limit in Eq. (60) with $r^2\omega^2/\ell^2c^2\to0$, then $\xi\to1$ [Eq. (54)], $S_3\to1$ [Eq. (59)], $\hat{E}_r\to-\partial\hat{\phi}/\partial r$ [Eq. (55)], and Eq. (60) simplifies to give the familiar form[13]

$$\frac{1}{r}\frac{\partial}{\partial r}\left(S_1 r \frac{\partial \hat{\phi}}{\partial r}\right) - \frac{\ell^2}{r^2} S_1 \hat{\phi}$$

$$= \frac{\ell}{r}\hat{\phi}\frac{\partial}{\partial r} S_2 + 4\pi\sigma_b \delta(r-R_0) \ . \tag{61}$$

Of course, strictly speaking, the electrostatic eigenvalue equation in Eq. (61) is valid only for a low-beta layer-plasma system with negligible magnetic field depression.

B. Approximate Eigenvalue Equation

For a layer-plasma system with arbitrary degree of field reversal, the electrostatic eigenvalue equation (61) is not valid and it is necessary to make use of Eq. (60). For the low-frequency ($\omega \sim \ell\omega_\theta$) perturbations considered here, it follows that

$$\left|\frac{\omega r}{\ell c}\right|^2 \approx \frac{R_0^2 \omega_\theta^2}{c^2} << 1 \ , \tag{62}$$

and hence that ξ can be approximated by

$$\xi \simeq 1 \tag{63}$$

in Eq. (60). On the other hand, for arbitrary degree of field reversal, it is necessary to retain terms proportional to $(\omega r/\ell c)^2 \sum_j \omega_{pj}^2/\nu_j^2$. We therefore approximate Eq. (60) by

$$\frac{1}{r}\frac{\partial}{\partial r}\left(\frac{S_1}{S_3} r \frac{\partial \hat{\phi}}{\partial r}\right) - \frac{\ell^2}{r^2}\frac{S_1}{S_3}\left[1 - \left(\frac{\omega r}{\ell c}\right)^2\left(\frac{S_2^2}{S_1} - S_1\right)\right]\hat{\phi}$$

$$= \frac{\ell}{r}\hat{\phi}\frac{\partial}{\partial r}\left(\frac{S_2}{S_3}\right) + 4\pi\sigma_b \delta(r-R_0) \ , \tag{64}$$

where S_1 and S_2 are defined in Eq. (59), and

$$S_3 \simeq 1 + \left(\frac{\omega r}{\ell c}\right)^2 \sum_j \frac{\omega_{pj}^2(r)}{\nu_j^2} \ . \tag{65}$$

The eigenvalue equation (64) is generally difficult to solve analytically. However, a formal dispersion relation that determines the complex eigenfrequency ω can be obtained in a relatively straightforward manner. Since the perturbed azimuthal electric field $\hat{E}_{\ell\theta}(r)$ is continuous across the layer ($r=R_0$), the function $\hat{\phi}(r)$ is also continuous at $r=R_0$. A further boundary condition on $\hat{\phi}(r)$ in Eq. (65) is determined from the discontinuity of $(\partial\hat{\phi}/\partial r)$ at $r=R_0$. For convenience of the subsequent analysis, we define the wave admittance $b_\pm$ as

$$b_-=(r\partial\hat{\phi}/\partial r)_{r=R_0^-}/\ell\hat{\phi}(R_0) \ ,$$
$$b_+=-(r\partial\hat{\phi}/\partial r)_{r=R_0^+}/\ell\hat{\phi}(R_0) \ , \tag{66}$$

where $R_0^\pm$ denotes $\lim_{\delta\to 0+}(R_0\pm\delta)$. Multiplying Eq. (64) by r and integrating with respect to r from $R_0-\delta$ to $R_0+\delta$ (with $\delta\to 0_+$) gives

$$\frac{2\ell c^2\nu/R_0^2}{(\omega-\ell\omega_\theta)^2-\ell^2\omega_r^2(a/R_0)^2} = -D^{-1}(\omega) \ , \tag{67}$$

where $D(\omega)$ is defined by

$$D^{-1}(\omega) = \frac{b_+S_1(R_0^+,\omega)+S_2(R_0^+,\omega)}{S_3(R_0^+,\omega)} + \frac{b_-S_1(R_0^-,\omega)-S_2(R_0^-,\omega)}{S_3(R_0^-,\omega)} \ , \tag{68}$$

and use has been made of the definition of σ_b [Eq. (47)].

Equation (67) constitutes the desired dispersion relation for the complex eigenfrequency ω. In order to evaluate closed expressions for $b_\pm$, however, we emphasize that it is necessary to solve Eq. (64) for the eigenfunction $\hat{\phi}(r)$. Although this generally requires a numerical analysis of Eq. (64), in Sec. V analytic

solutions for $\hat{\phi}(r)$ are obtained in two limiting regimes of experimental interest.

In concluding this section, it is instructive to solve Eq. (67) iteratively for eigenfrequency ω in the vicinity of $\ell\omega_\theta$. If it is valid to approximate $\omega \simeq \ell\omega_\theta$ on the right-hand side of Eq. (67), we obtain

$$(\omega-\ell\omega_\theta)^2 = \ell^2\omega_r^2 \frac{a^2}{R_0^2} - 2\ell \frac{\nu c^2}{R_0^2} D(\ell\omega_\theta) \quad . \tag{69}$$

Making use of $\omega_r^2 = v_i^2/a^2 = 2\hat{T}/m_i a^2$ [Eq. (23)], it follows from Eq. (69) that

$$2\ell\nu D(\ell\omega_\theta) > v_i^2/c^2 \tag{70}$$

is a necessary and sufficient condition for instability.

Equation (69) constitutes one of the main results of this paper and can be used to investigate stability properties for a broad range of system parameters. In this regard, we emphasize that Eq. (69) has been derived with no a priori assumption regarding the size of the electromagnetic coupling parameter

$$K = \left(\frac{\omega R_0}{\ell c}\right)^2 \sum_j \frac{\omega_{pj}^2(r)}{\omega_{cj}^2(r)} \quad . \tag{71}$$

For general value of K, the eigenvalue equation (64) must be solved numerically to determine the wave admittances $b_\pm$ [Eq. (66)]. However, in the limiting regimes where $|K| \ll 1$ or $|K| \gg 1$, closed analytic expressions for $\hat{\phi}(r)$ (and hence $b_\pm$) can be obtained in a straightforward manner.

For a low-density background plasma consistent with $|K| \ll 1$, the electrostatic approximation is valid and the corresponding stability properties[13] have been investigated previously by the authors for a weakly diamagnetic configuration. In the subsequent analysis, we therefore

investigate stability properties for a high-density background plasma with $|K|>>1$ for $0<r<R_0$, and arbitrary degree of field reversal.

V. STABILITY ANALYSIS FOR A HIGH-DENSITY BACKGROUND PLASMA

A. Eigenvalue Equation

In this section, we obtain closed expressions for the wave admittance $b_{\pm}$ [Eq. (66)], and the results are used to investigate the dispersion relation in Eq. (67). Making use of $\xi \simeq 1$ and Eqs. (53) and (56), it is straightforward to show from Eq. (64) that the eigenfunction $\hat{\phi}(r)$ satisfies

$$\left\{ \frac{1}{r}\frac{\partial}{\partial r} r \frac{\partial}{\partial r} - \frac{2}{r}\left(1 - \frac{1}{S_3}\right)\frac{\partial}{\partial r} - \frac{\ell^2}{r^2}\left[1 - \frac{2S_2}{\ell S_1}\left(1 - \frac{1}{S_3}\right)\right] + \left(\frac{\omega}{c}\right)^2 \left(\frac{S_2^2}{S_1} - S_1\right) \right\} \hat{\phi}(r) = 0 \ , \tag{72}$$

at all radial points except $r=R_0$. In the limiting regimes where $|K| \ll 1$ or $|K| \gg 1$, the eigenvalue equation (72) can be simplified to give

$$\left(\frac{1}{r}\frac{\partial}{\partial r} r \frac{\partial}{\partial r} - \frac{\ell^2}{r^2}\right)\hat{\phi}(r) = 0 \ , \quad |K| \ll 1 \ ,$$

$$r \frac{\partial}{\partial r}\frac{1}{r}\frac{\partial}{\partial r} - \frac{\ell^2}{r^2}\left(1 - \frac{2S_2}{\ell S_1}\right) + \frac{\omega^2}{c^2}\left(\frac{S_2^2}{S_1} - S_1\right)\hat{\phi}(r) = 0 \ , \quad |K| \gg 1 \ , \tag{73}$$

where use has been made of $S_3 \simeq 1$ for $|K| \ll 1$, and $S_3 \gg 1$ for $|K| \gg 1$. For $\omega_{pi}^2/\omega_{ci}^2 \gg 1$ and $m_i/m_e \gg 1$, the quantities S_1 and S_2 in Eq. (73) can be approximated by

$$S_2 \simeq \frac{\omega}{\omega_{ci}(r)} S_1 \simeq \frac{\omega}{\omega_{ci}(r)} \frac{\omega_{pi}^2(r)}{\nu_i^2(r)} \ , \tag{74}$$

provided $(1-\nu)^2 \gg (\ell m_e/m_i)^2$. [This is a very weak limitation on the range of ν for which the subsequent stability analysis is valid. It essentially allows for all values in the range $0<\nu<\infty$, except $\nu=1$.] Substituting Eq. (74) into Eq. (73), we obtain

$$\left[r \frac{\partial}{\partial r} \frac{1}{r} \frac{\partial}{\partial r} - \frac{\ell^2}{r^2} \left(1 - \frac{2\omega}{\ell \omega_{ci}(r)} \right) + \frac{\omega^2}{c^2} \frac{\omega_{pi}^2}{\omega_{ci}^2(r)} \right] \hat{\phi}(r)=0 \ , \tag{75}$$

for $|K|>>1$.

From Eq. (37), it is straightforward to express Eq. (75) as

$$\left(\frac{1}{r} \frac{\partial}{\partial r} r \frac{\partial}{\partial r} - \frac{q^2}{r^2} + p^2 \right) \hat{E}_\theta(r)=0 \ , \tag{76}$$

where

$$\begin{aligned} p &= - \frac{\omega \omega_{pi}(r)}{c|\omega_{ci}(r)|} \ , \\ q &= \left\{ 1+\ell^2 \left[1 - \frac{2\omega}{\ell \omega_{ci}(r)} \right] \right\}^{1/2} \ . \end{aligned} \tag{77}$$

In obtaining Eq. (76), use has been made of the property that $\omega_{pi}(r)$ and $\omega_{ci}(r)$ are uniform except at $r=R_0$ [see Eqs. (53) and (56)]. The solution to Eq. (76) is a linear combination of $J_q(pr)$ and $N_q(pr)$, where $J_q(pr)$ and $N_q(pr)$ are the Bessel functions of the first and second kind, respectively. In the subsequent analysis, it is convenient to express Budker's parameter (ν) and the angular velocity (ω_θ) in terms of the compression ratio η [see Eqs. (25) and (26)]

$$\begin{aligned} \nu &= (1-\eta)/(1+\eta) \ , \\ \omega_\theta / \hat{\omega}_{ci} &= -(1+\eta)/2 \ . \end{aligned} \tag{78}$$

B. Rectangular Plasma Density Profile ($\alpha=0$)

As a simple limiting case, we examine stability properties in circumstances where the plasma density outside the layer is identically zero, i.e.,

$$\alpha = 0 \ . \tag{79}$$

In the vacuum region ($R_0<r<R_c$), it follows that $|K|<<1$ and the solution for $\hat{\phi}(r)$ has the simple form [Eq. (73)]

$$\hat{\phi}(r)=\hat{\phi}(R_0)\ \frac{(R_0/r)^{\ell}-(R_0 r/R_c^2)^{\ell}}{1-(R_0/R_c)^{2\ell}}\ , \quad R_0<r<R_c \ . \tag{80}$$

The wave admittance b_+ can be determined by substituting Eq. (80) into Eq. (66) which gives

$$b_+=(R_c^{2\ell}+R_0^{2\ell})/(R_c^{2\ell}-R_0^{2\ell}) \ . \tag{81}$$

For a dense background plasma core with $|K|>>1$ in the range $0<r<R_0$, the wave admittance b_- is determined by solving Eq. (76) for $\hat{\phi}(r)$. Approximating $\omega\simeq\ell\omega_\theta$ in Eq. (77) and making use of Eqs. (53) and (78), we find that the index q can be expressed as (for $0<r<R_0$)

$$q\simeq[1+\ell^2(2+1/\eta)]^{1/2} \ .$$

For analytic simplicity, q is assumed to be real in the subsequent analysis, which restricts η to the range

$$\begin{aligned} &0<\eta<1 \ , \quad \text{for } \eta>0 \ , \\ &-1<\eta<-\ell^2/(1+2\ell^2), \quad \text{for } \eta<0 \ . \end{aligned} \tag{82}$$

Within the context of Eq. (82), the physically acceptable solution to Eq. (76) can be expressed as

$$\hat{E}_\theta(r)=AJ_q(pr), \quad 0<r<R_0 \ , \tag{83}$$

where A is an arbitrary constant, $p=-(\omega/c)(\hat{\omega}_{pi}/|\eta|\hat{\omega}_{ci})$, and $\hat{\omega}_{pi}=(4\pi n_p e^2/m_i)^{1/2}$ is the ion plasma frequency. Substituting Eqs. (37)

and (83) into Eq. (66) yields

$$b_-(\omega) = \frac{1}{\ell}\left[1 + \frac{pR_0 J_q'(pR_0)}{J_q(pR_0)}\right] , \tag{84}$$

where the prime (') denotes (1/p)d/dr.

After some straightforward algebraic manipulation of Eqs. (59), (68), (81), and (84), the dispersion relation is given by

$$\frac{2\ell c^2 \nu/R_0^2}{(\omega-\ell\omega_\theta)^2-\ell^2\omega_r^2(a/R_0)^2} = \frac{R_c^{2\ell}+R_0^{2\ell}}{R_c^{2\ell}-R_0^{2\ell}} + \left(\frac{\ell c}{\omega R_0}\right)^2\left[\frac{\omega}{\eta\hat{\omega}_{ci}} - \frac{1}{\ell} - \frac{pR_0 J_q'(pR_0)}{\ell J_q(pR_0)}\right] , \tag{85}$$

where ν and ω_θ can be eliminated in favor of the reversal parameter η by Eq. (78).

For a dense background plasma with $|K|_{r=R_0^-} = |p^2R_0^2| >> 1$, it is evident that the term proportional to J_q'/J_q dominates on the right-hand side of Eq. (85). In this regard, we approximate Eq. (85) by

$$\frac{2\ell\nu c/R_0}{(\omega-\ell\omega_\theta)^2-\ell^2\omega_r^2(a/R_0)^2} = -\frac{2\hat{\omega}_{pi}}{\eta(1+\eta)\hat{\omega}_{ci}}\left(\frac{J_q'}{J_q}\right) , \tag{86}$$

where $\hat{\omega}_{pi}=(4\pi n_p e^2/m_i)^{1/2}$, $\hat{\omega}_{ci}=eB_0/m_i c$, and use has been made of Eqs. (53), (56), (77), and (78), and $\omega \simeq \ell\omega_\theta$.

For convenience of notation in the subsequent analysis, we introduce the dimensionless quantities

$$\zeta = \frac{a\hat{\omega}_{pi}}{c}\left(\frac{J_q'}{J_q}\right)_{\omega=\ell\omega_\theta} ,$$
$$\zeta' = \frac{a\hat{\omega}_{pi}\hat{\omega}_{ci}}{c}\left[\frac{d}{d\omega}\left(\frac{J_q'}{J_q}\right)\right]_{\omega=\ell\omega_\theta} , \tag{87}$$

and the normalized Doppler-shifted complex eigenfrequency

$$\Omega=(\omega-\ell\omega_\theta)/\hat{\omega}_{ci} . \tag{88}$$

The quantity $\omega_r^2 a^2/R_0^2 = 2\hat{T}/m_i R_0^2$ occurring in Eq. (87) can be expressed in terms of the reversal parameter η by making use of Eqs. (22), (23), and (78). After some straightforward algebra, we obtain

$$\omega_r^2 a^2/R_0^2 = \hat{\omega}_{ci}^2 (a/R_0)(1-\eta^2)/4 \ . \tag{89}$$

Substituting Eqs. (87)-(89) into Eq. (86), and Taylor-expanding (J_q'/J_q) in Eq. (86) about $\omega = \ell\omega_\theta$, we obtain the dispersion relation

$$\frac{\zeta'}{\zeta}\,\Omega^3 + \Omega^2 - \ell\lambda\,\frac{\zeta'}{\zeta}\,\Omega + 2\lambda\left(\frac{2\eta}{\zeta(1+\eta)} - \frac{\ell}{2}\right) = 0 \ , \tag{90}$$

where

$$\lambda = \frac{\ell a}{R_0}\,\frac{1-\eta^2}{4} \ . \tag{91}$$

The parameter ζ in Eq. (90) is an oscillatory function of plasma density. It is evident from Eq. (90) that the parameter ζ plays a decisive role in determining stability behavior. Moreover, the system can be stabilized by increasing the azimuthal harmonic number ℓ, since the terms proportional to ℓ in Eq. (90) have a stabilizing influence. The stabilization associated with sufficiently large ℓ is provided by the effective transverse temperature ($\hat{T}$) of the layer ions, and hence is associated with the finite layer thickness $a = (2\hat{T}/m_i\omega_r^2)^{1/2}$ [Eq. (23)]. Moreover, shown in Eq. (32), the quantity $\hat{T}$ is directly related to the canonical angular momentum spread (Δ) for the class of rigid-rotor Vlasov equilibria described by Eq. (2). Therefore, the stabilization provided by the transverse temperature $\hat{T}$ is also associated with the finite spread in canonical angular momentum.[11] This effect is most pronounced when the reversal parameter η is close to zero [Eq. (90)].

Specific stability properties, determined numerically from Eq. (90), will be discussed in Sec. V.C.

C. Stability Analysis for Arbitrary α

In this section, we investigate stability properties for the case where the plasma density outside the ion layer ($R_0<r<R_c$) is sufficiently high that

$$\alpha\left|\frac{\omega^2R_0^2}{\ell^2c^2}\right|\frac{\hat{\omega}_{pi}^2}{\hat{\omega}_{ci}^2}=\alpha\eta^2|K|_{r=R_0^-}$$
$$=|K|_{r=R_0^+}\gg 1\ . \tag{92}$$

Here $\hat{\omega}_{ci}=eB_0/m_ic$ is the ion cyclotron frequency, αn_p is the plasma density outside the layer, and $\alpha\hat{\omega}_{pi}^2=4\pi\alpha n_pe^2/m_i$ is the associated ion plasma frequency-squared. The required solution to Eq. (76) in the range $R_0<r<R_c$ is given by

$$\hat{E}_\theta(r)=B[J_q(pr)N_q(pR_c)-J_q(pR_c)N_q(pr)]\ , \tag{93}$$

where B is a constant and use has been made of the boundary condition $\hat{E}_\theta(r=R_c)=0$. Substituting Eqs. (37) and (93) into Eq. (66) yields

$$b_+(\omega)=-\frac{1}{\ell}+\frac{pR_0}{\ell}\frac{J_q(pR_c)N_q'(pR_0)-J_q'(pR_0)N_q(pR_c)}{J_q(pR_0)N_q(pR_c)-J_q(pR_c)N_q(pR_0)}\ . \tag{94}$$

The dispersion relation can be derived by substituting Eqs. (84) and (94) into Eq. (68). After some straightforward algebraic manipulation, we obtain the approximate dispersion relation

$$\frac{2\omega^2\nu}{(\omega-\ell\omega_\theta)^2-\ell^2\omega_r^2(a/R_0)^2}=-\ell(b_-+b_+)\ , \tag{95}$$

where the sum of the wave admittances, (b_-+b_+), can be approximated by

$$b_-(\omega)+b_+(\omega) = \frac{p_-R_0J'_{q-}(p_-R_0)}{\ell J_{q-}(p_-R_0)}$$
$$+\left(\frac{p_+R_0}{\ell}\right)\frac{J_{q+}(p_+R_c)N'_{q+}(p_+R_0)-J'_{q+}(p_+R_0)N_{q+}(p_+R_c)}{J_{q+}(p_+R_0)N_{q+}(p_+R_c)-J_{q+}(p_+R_c)N_{q+}(p_+R_0)} . \tag{96}$$

In Eq. (96), $p_-=-(\omega/c)(\hat{\omega}_{pi}/|\eta|\hat{\omega}_{ci})$, $p_+=-(\omega/c)(\alpha^{1/2}\hat{\omega}_{pi}/\hat{\omega}_{ci})=|\eta|\alpha^{1/2}p_-$, $q_-\simeq[1+\ell^2(2+1/\eta)]^{1/2}$, and $q_+\simeq[1+\ell^2(2+\eta)]$. In deriving Eq. (95), use has been made of Eqs. (65), (74), and (92). Moreover, in obtaining the expressions for $q_\pm$, use has been made of Eq. (77), and $\omega\simeq\ell\omega_\theta=-\ell(1+\eta)\hat{\omega}_{ci}/2$. Since the eigenfrequency ω is very close to $\ell\omega_\theta$, we Taylor-expand the right-hand side of Eq. (95) about $\omega=\ell\omega_\theta$, retaining terms to first order in $(\omega-\ell\omega_\theta)$. After some straightforward algebra, Eq. (98) can be approximated by

$$\frac{2\ell\omega_\theta^2\nu}{(\omega-\ell\omega_\theta)^2-\ell^2\omega_r^2(a/R_0)^2} = -[b_-(\omega)+b_+(\omega)]_{\omega=\ell\omega_\theta}$$
$$-\left[\frac{d}{d\omega}(b_-+b_+)\right]_{\omega=\ell\omega_\theta}(\omega-\ell\omega_\theta) , \tag{97}$$

where ω_θ and $\omega_r^2(a/R_0)^2$ are defined in Eqs. (78) and (89), respectively.

The growth rate $\gamma=\mathrm{Im}\omega$ and real oscillation frequency $\mathrm{Re}\omega$ have been obtained numerically from the cubic dispersion relation (97) for a broad range of system parameters η, $\hat{\omega}_{pi}R_0/c$, α, ℓ, and R_0/R_c. In the remainder of this section, we summarize several features of the stability properties determined from Eq. (97). From Eqs. (41) and (78), the real frequency $\mathrm{Re}\omega$ can be approximated by

$$\mathrm{Re}\omega\simeq\ell\omega_\theta=-\ell(1+\eta)\hat{\omega}_{ci}/2 . \tag{98}$$

The real frequency $\mathrm{Re}\omega$ determined numerically from Eq. (97) is very close to the value in Eq. (98). In this context, we only present numerical results for the instability growth rate γ.

In order to illustrate the dependence of stability properties on the degree of field reversal, we calculate the wave admittances and the instability growth rate. Shown in Fig. 6(a) is a plot of $(b_-+b_+)_{\omega=\ell\omega_\theta}$ versus η, for $\ell=2$, $\hat{\omega}_{pi}R_0/c=4$ and $\alpha=0$. [In the limiting case of no plasma outside the ion layer ($\alpha=0$), the dispersion relation (97) reduces identically to the dispersion relation (90) obtained in Sec. V.B.] It is evident from Fig. 6(a) that the curves representing $(b_-+b_+)_{\omega=\ell\omega_\theta}$ become more vertical and the distance between curves decreases rapidly as η decreases (or, equivalently, as Budker's parameter ν increases). For $\eta<0.3$, it is readily shown that $(b_-+b_+)_{\omega=\ell\omega_\theta}$ can be approximated by

$$(b_-+b_+)_{\omega=\ell\omega_\theta}=(b_-)_{\omega=\ell\omega_\theta}\simeq -\left(\frac{2(1-\eta)}{\eta}\right)\tan\left[\frac{4(1-\eta)}{\eta}-\frac{\pi}{2}\left(1+4/\eta\right)^{1/2}-\frac{\pi}{4}\right], \tag{99}$$

for the parameters in Fig. 6(a). In obtaining Eq. (99), use has been made of Eq. (77) and $J_n(x)\simeq(2/\pi x)^{1/2}\cos(x-n\pi/2-\pi/4)$ for large x. Equation (99) provides a good description of the behavior in Fig. 6(a). In this regard, we do not plot (b_-+b_+) for $\eta<0.2$. Figure 6(b) shows a plot of the normalized growth rate $\gamma/\hat{\omega}_{ci}$ versus η obtained from Eq. (97) for $\alpha=0$, $R_0/R_c=0.5$, $a/R_0=0.05$, and parameters otherwise identical to Fig. 6(a). Several points are noteworthy in Fig. 6(b). First, the system is stabilized when the reversal parameter η approaches zero. This feature has been predicted analytically in Sec. V.B. Second, the growth rate curve exhibits a repetitive behavior, with the maximum growth rate for each unstable zone decreasing as η decreases. Third, the maximum growth rate for each zone occurs at a value of η corresponding to $(b_-+b_+)_{\ell\omega_\theta}\simeq 0$ [Figs. 6(a) and (b)]. Finally, when instability does exist, the maximum growth rate can be a substantial fraction of ion cyclotron frequency $\hat{\omega}_{ci}$.

Shown in Fig. 7(a) for ℓ=2 and in Fig. 7(b) for ℓ=4 are plots of normalized growth rate $\gamma/\hat{\omega}_{ci}$ versus the reversal parameter η [Eq. (97)] for α=0.2 and parameters otherwise identical to Fig. 6(b). Comparing Figs. 7(a) and 6(b), we note that the stability properties are almost identical for α=0 and α=0.2, although the maximum growth rate does decrease slowly as α increases. We therefore conclude that the influence of plasma outside the layer on stability behavior is weak, at least when α is sufficiently small ($\alpha \lesssim 0.5$, say). Moreover, we also note from Fig. 7 that the width of the instability zones is reduced for increasing values of azimuthal harmonic number ℓ. Furthermore, high-harmonic perturbations are easily stabilized as η approaches zero.

The dependence of stability properties on plasma density is illustrated in Fig. 8(a) for ℓ=2 and in Fig. 8(b) for ℓ=4, where the normalized growth rate $\gamma/\hat{\omega}_{ci}$ is plotted versus $\hat{\omega}_{pi}R_0/c$ for η=0.82 and parameters otherwise identical to Fig. 7. Note that the growth rate is a decreasing function of $\hat{\omega}_{pi}R_0/c$. This feature is also evident from Eqs. (87) and (90) for α=0. We further note from Fig. 8(b) that the system is completely stabilized above some critical value of $\hat{\omega}_{pi}R_0/c$. For example, from Fig. 8(b), the ℓ=4 perturbation is stable for $\hat{\omega}_{pi}R_0/c \gtrsim 7$. In this regard, we conclude that the layer-plasma configuration can be completely stabilized provided the plasma density is sufficiently high.

Of considerable interest for experimental application is the stability behavior for a field-reversed configuration with η<0. Figure 9 shows a plot of normalized growth rate versus η obtained from Eq. (97) for ℓ=2 [Fig. 9(a)] and ℓ=4 [Fig. 9(b)], and equilibrium parameters $\hat{\omega}_{pi}R_0/c$=10, α=0.2, R_0/R_c=0.5, and a/R_0=0.05. As discussed in Sec. V.B,

for $\eta<0$, Eq. (97) is valid only when $-1<\eta<-\ell^2/(1+2\ell^2)$ [Eq. (82)], and $|K|_{r=R_0^-}>>1$. Moreover, the electromagnetic coupling parameter $|K|_{r=R_0^-}$ decreases to zero when η approaches minus unity. In this regard, the plots in Fig. 9 are presented only for the range $-0.85<\eta<-0.5$. We note from Figs. 9(a) and 9(b) that the instability growth rate decreases considerably as $|\eta|$ approaches 0.5. The stabilization for low value of $|\eta|$ is associated with finite beta electromagnetic effects. Moreover, this stabilization is most pronounced for high azimuthal harmonic numbers [compare Figs. 9(a) and (b)]. We conclude from Figs. 7 and 9 that the system is most stable when the magnetic compression ratio η approaches zero.

VI. NUMERICAL ANALYSIS OF STABILITY PROPERTIES FOR ARBITRARY VALUES OF BACKGROUND PLASMA DENSITY

In this section, we investigate the stability properties numerically for arbitrary values of background plasma density, assuming a rectangular density profile with $\alpha = 0$. As shown in Sec. V.A, the eigenfunction $\hat{\phi}(r)$ for arbitrary n_p satisfies Eq. (72) at all radial locations, except at $r = R_0$. Since the stability analysis in this section is limited to $\alpha = 0$, the wave admittance b_+ is given by Eq. (81). However, in order to determine the wave admittance b_- in the region $0 < r < R_0$, it is necessary to solve the eigenvalue equation (72), which is a simple second-order differential equation with boundary conditions $\hat{\phi}(r=0) = (d\hat{\phi}/dr)_{r=0} = 0$ at $r = 0$.

The eigenfunction $\hat{\phi}(r)$ has been calculated numerically Eq. (72) for $\ell = 2$ and $\omega \simeq -\ell\hat{\omega}_{ci}$, which corresponds to full reversal with $\eta \simeq 1$. Shown in Fig. 10 are the corresponding plots of $\hat{\phi}(r)$ versus r/R_0 for (a) $\hat{\omega}_{pi}R_0/c=1$, (b) $\hat{\omega}_{pi}R_0/c=5$, and (c) $\hat{\omega}_{pi}R_0/c=10$. It is evident from Fig. 10(a) that the electrostatic eigenfunction $\hat{\phi}(r) = (r/R_0)^{\ell}$ is a very good approximation for a low-density background plasma satisfying $\hat{\omega}_{pi}R_0/c \lesssim 1$. However, for a high-density background plasma with $\hat{\omega}_{pi}R_0/c > 1$, the eigenfunction exhibits oscillatory (Bessel-function-like) behavior, which indicates the important influence of electromagnetic effects associated with background plasma dielectric properties [Fig. 10(b) and (c)]. Moreover, the eigenfunction oscillates rapidly as a function of increasing plasma density. In order to illustrate the dependence of the wave admittance $b_- = R_0(d\hat{\phi}/dr)_{R_0}/\ell\hat{\phi}(R_0)$ on plasma density, Fig. 11 shows a plot of b_- versus $\hat{\omega}_{pi}R_0/c$ for $\ell=2$ and $\eta=1$. Evidently, from Fig. 11, the wave admittance b_- is approximately equal to unity in the range $0 < \hat{\omega}_{pi}R_0/c<1$, thereby ensuring that the electrostatic

approximation is valid for a low-density background plasma. On the other hand, it is also clear from Fig. 11 that electromagnetic effects are very important for plasma densities satisfying $\hat{\omega}_{pi}R_0/c \gtrsim 2$.

The dependence of stability properties on plasma density is illustrated in Fig. 12, where the normalized growth rate $\gamma/\hat{\omega}_{ci}$ is plotted versus $\hat{\omega}_{pi}R_0/c$ for $\ell=2$, and $\eta=0.95$[Fig. 12(a)] and $\eta= -0.9$ [Fig. 12(b)]. In Fig. 12(a), the stability properties are very similar to the results obtained analytically in Fig. 8(a). Moreover, for a highly field-reversed layer [Fig. 12(b)], it is evident that the instability can be completely stabilized by increasing the plasma density beyond a certain critical value [$\hat{\omega}_{pi}R_0/c=20.5$ in Fig. 12(b)]. Shown in Fig. 13 is a plot of growth rate $\gamma/\hat{\omega}_{pi}$ versus η for $\ell=2$ and $\hat{\omega}_{pi}R_0/c=10$. As expected from the analytic results in Figs. 7(a) and 9(a), for $|\eta| \lesssim 0.4$, the instability is completely stabilized by the effects of finite transverse temperature of the layer ions. Finally, comparing Figs. 12 and 13 with the results obtained analytically in Sec. V.C, we conclude that the analytic studies in Sec. V.C give a good qualitative description of stability behavior.

VII. CONCLUSIONS

In this paper, we have investigated the electromagnetic stability properties of an intense P-layer immersed in a dense plasma background. The equilibrium and stability analysis was carried out within the framework of a hybrid Vlasov-fluid model in which the background plasma electrons and ions are described as macroscopic, cold fluids confined by the axial magnetic field $B_z^0(r)\hat{e}_z$, and the layer ions are described by the Vlasov equation. Moreover, the equilibrium and stability properties were calculated for the case in which the background plasma has a step-function density profile and the layer ions are described by the rigid-rotor distribution function in Eq. (2). Various equilibrium properties were calculated in Sec. II. One of the most important features in the equilibrium analysis for a thin layer is that Budker's parameter ν for the layer ions is directly related to the magnetic compression ratio η by $\nu=(1-\eta)/(1+\eta)$. Electromagnetic stability properties were investigated in Secs. III-VI, assuming that all perturbed quantities are independent of axial coordinate ($\partial/\partial z=0$). A formal stability analysis was carried out in Sec. IV. Equation (69), when combined with Eq. (68), constitute one of the main results of this paper and can be used to investigate stability properties for a broad range of system parameters. A detailed analytic and numerical investigation of electromagnetic stability properties was carried out in Sec. V for a dense background plasma and in Sec. VI for arbitrary values of background plasma density. It was found that the effects of (a) the equilibrium magnetic field depression produced by the P-layer, (b) transverse magnetic perturbations ($\delta\underset{\sim}{B}\neq 0$), (c) small (but finite) transverse temperature of the layer ions, and (d) the dielectric properties of the background plasma, all have

an important influence on stability behavior. For example, for a dense background plasma, the system can be easily stabilized by a sufficiently large transverse temperature of the layer ions.

ACKNOWLEDGMENTS

This research was supported by the National Science Foundation. The research by one of the authors (H.S.U.) was supported in part by the Office of Naval Research.

APPENDIX A

EVALUATION OF PERTURBED CHARGE DENSITY FOR THE LAYER IONS

To complete the stability analysis, in this Appendix we evaluate the perturbed charge density associated with the layer ions. Combining Eqs. (3) and (43), it is straightforward to show that the radial equation of motion for the layer ions is given by

$$r'-r=(v_\perp/\omega_r)[\cos(\omega_r\tau-\alpha)-\cos\alpha] \ , \qquad (A.1)$$

where $\tau=t'-t$, $v_\perp$ is the perpendicular speed in a frame of reference rotating with angular velocity ω_θ, $\cos\alpha=(v_\theta-r\omega_\theta)/v_\perp$, and r' and r are the radial distances of the particles from the z-axis at times $t'=t'$ and $t'=t$, respectively. The time derivative of Eq. (A.1) gives the radial velocity,

$$v_r'=v_\perp(\sin\alpha\cos\omega_r\tau-\cos\alpha\sin\omega_r\tau) \ , \qquad (A.2)$$

for the layer ions.

Consistent with Eq. (1), the perturbed distribution function for a thin ion layer can be expressed as,

$$\hat{f}_{b\ell}(r,\underset{\sim}{v})=e\frac{\partial f_b^0}{\partial U}\int_{-\infty}^{0}d\tau\ \exp\{-i(\omega\tau-\ell(\theta'-\theta))\}$$
$$\times\left\{\frac{v_\perp}{R_0}\cos\alpha\left[i\ell\hat{\phi}(R_0)+\frac{R_0v_r'}{c}\hat{B}_{\ell z}(R_0)\right]+\left(\frac{\partial\hat{\phi}}{\partial r}\right)_{R_0}v_r'\right\} \ , \qquad (A.3)$$

where use has been made of Eqs. (38), (40), and (42). Since the variable $(\theta'-\theta)$ in Eq. (A.3) is a function of $\cos\alpha$, it follows from Eqs. (46), (A.2), and (A.3) that any term in the time integration in Eq. (A.3) that is a function of $\sin\alpha$ will give zero when the integration over α is carried out. In this context, we can replace Eq. (A.2) by

$$v_r' = -v_\perp \cos\alpha \sin\omega_r\tau \ , \tag{A.4}$$

without loss of generality in the present analysis. For low-frequency ($\omega \sim \ell\omega_\theta$) perturbations, consistent with Eqs. (41) and (63), it is valid to neglect the term proportional to $\hat{B}_{\ell z}(R_0)$ in Eq. (A.3), since the corrections associated with this term are of order $|\omega-\ell\omega_\theta|/\hat{\omega}_{ci}$ ($<<1$) or smaller than the corrections associated with the term proportional to $(\partial\hat{\phi}/\partial r)_{R_0}$ in Eq. (A.3). This can be easily verified by making use of Eqs. (36), (55), and (A.4). Substituting Eq. (A.4) into Eq. (A.3), we obtain an approximate expression for the perturbed distribution function,

$$\hat{f}_{b\ell}(r,\underset{\sim}{v}) = i\ell\cos\alpha \, \frac{v_\perp}{R_0} \frac{\partial f_b^0}{\partial U} \int_{-\infty}^{0} d\tau \, \exp\{-i[\omega\tau-\ell(\theta'-\theta)]\}$$
$$\times \left\{\hat{\phi}(R_0)+\left[R_0\left(\frac{\partial\hat{\phi}}{\partial r}\right)_{R_0}/2\ell\right][\exp(i\omega_r\tau)-\exp(-i\omega_r\tau)]\right\} . \tag{A.5}$$

The perturbed surface charge density $\sigma_{b\ell}$ for a very thin ion layer is evaluated by substituting Eqs. (42) and (A.5) into Eq. (46). After some straightforward algebra, we obtain

$$\sigma_{b\ell} = \frac{1}{2\pi} \frac{\nu\ell^2 c^2}{R_0^3} \left[\frac{\hat{\phi}(R_0)}{(\omega-\ell\omega_\theta)^2-\ell^2\omega_r^2(a/R_0)^2} + \frac{2R_0}{\ell}\left(\frac{\partial\hat{\phi}}{\partial r}\right)_{R_0} \frac{(\omega-\ell\omega_\theta)}{\omega_r^3}\right] , \tag{A.6}$$

where use has been made of Eq. (41). From Eq. (A.6), it is easily shown that the correction associated with the term proportional to $(\partial\hat{\phi}/\partial r)_{R_0}$ is negligibly small except when $|R_0(\partial\hat{\phi}/\partial r)_{R_0}/\hat{\phi}(R_0)| \to \infty$. In this context, we conclude that the perturbed surface charge density $\sigma_{b\ell}$ for a thin ion layer can be approximated by,

$$\sigma_{b\ell} = \frac{1}{2\pi} \frac{\nu\ell^2 c^2 \hat{\phi}(R_0)/R_0^3}{(\omega-\ell\omega_\theta)^2-\ell^2\omega_r^2(a/R_0)^2} . \tag{A.7}$$

REFERENCES

1. H. A. Davis, R. A. Meger, and H. H. Fleischmann, Phys. Rev. Lett. 37, 542 (1976).
2. S. C. Luckhardt and H. H. Fleischmann, Phys. Rev. Lett. 39, 747 (1977).
3. R. N. Sudan and E. Ott, Phys. Rev. Lett. 33, 355 (1974).
4. C. A. Kapetanakos, J. Golden, and K. R. Chu, Plasma Phys. 19, 387 (1977).
5. H. A. Davis, H. H. Fleischmann, R. E. Kribel, D. Larrabee, R. V. Lovelace, S. C. Luckhardt, D. Rej, and M. Tuszewski, in Proceedings 2nd International Topical Conference on High Power Electron and Ion Beam Research and Technology (Ithaca, N. Y. 1977), Vol. I, p. 423.
6. C. A. Kapetanakos, J. Golden, Adam Drobot, R. A. Mahaffey, S. J. Marsh, and J. A. Pasour, in Proceedings 2nd International Topical Conference on High Power Electron and Ion Beam Research and Technology (Ithaca, N. Y. 1977), Vol. I, p. 435.
7. A. Mohri, K. Narihara, T. Tsuzuki, and Y. Kubota, in Proceedings 2nd International Topical Conference on High Power Electron and Ion Beam Research and Technology (Ithaca, N. Y. 1977), Vol. I, p. 459.
8. D. E. Baldwin and M. E. Rensink, Comments on Plasma Physics and Controlled Fusion, in press (1978).
9. R. V. Lovelace, Phys. Rev. Lett. 35, 162 (1975).
10. R. N. Sudan and M. N. Rosenbluth, Phys. Rev. Lett. 36, 972 (1976).
11. H. Uhm and R. C. Davidson, Phys. Fluids 20, 771 (1977).
12. H. S. Uhm and R. C. Davidson, Phys. Fluids 21, 265 (1978).
13. H. S. Uhm and R. C. Davidson, "Stability Properties of a Cylindrical Rotating P-Layer Immersed in a Uniform Background Plasma", submitted for publication (1978).

FIGURE CAPTIONS

Fig. 1 Equilibrium configuration and coordinate system.

Fig. 2 Density profile [Eq. (9)] for the layer ions.

Fig. 3 Axial magnetic field profile [Eq. (14)].

Fig. 4 Sketch of the envelope function $\psi(r)$ versus r [Eq. (11)] with $\psi(R_1)=0=\psi(R_2)$ and $[\partial\psi/\partial r]_{r=R_0}=0$.

Fig. 5 Electron and ion density profiles [Eq. (44)] for the background plasma.

Fig. 6 Plots of (a) sum of wave admittances $(b_-+b_+)_{\omega=\ell\omega_\theta}$ [Eq. (96)] and (b) normalized growth rate $\gamma/\hat{\omega}_{ci}$ [Eq. (97)] versus η for $\ell=2$, $\hat{\omega}_{pi}R_0/c=4$, $\alpha=0$, $R_0/R_c=0.5$ and $a/R_0=0.05$.

Fig. 7 Plot of normalized growth rate $\gamma/\hat{\omega}_{ci}$ versus η [Eq. (97)] for $\alpha=0.2$. Cases shown are for (a) $\ell=2$ and (b) $\ell=4$, and parameters otherwise identical to Fig. 6.

Fig. 8 Plots of normalized growth rate $\gamma/\hat{\omega}_{ci}$ versus $\hat{\omega}_{pi}R_0/c$ [Eq. (97)] for (a) $\ell=2$ and (b) $\ell=4$, with $\eta=0.82$ and parameters otherwise identical to Fig. 7.

Fig. 9 Plots of normalized growth rate $\gamma/\hat{\omega}_{ci}$ versus η [Eq. (97)] for (a) $\ell=2$, and (b) $\ell=4$, with $\hat{\omega}_{pi}R_0/c=10$, $\alpha=0.2$, $R_0/R_c=0.5$ and $a/R_0=0.05$.

Fig. 10 Plot of eigenfunction $\hat{\phi}(r)$ versus r/R_0 [Eq. (72)] for $\ell=2$, $\eta=1$ and (a) $\hat{\omega}_{pi}R_0/c=1$, (b) $\hat{\omega}_{pi}R_0/c=5$, and (c) $\hat{\omega}_{pi}R_0/c=10$.

Fig. 11 Plot of wave admittance $b_-=R_0(d\hat{\phi}/dr)_{R_0}/\ell\hat{\phi}(R_0)$ versus $\hat{\omega}_{pi}R_0/c$ for $\ell=2$ and $\eta=1$.

Fig. 12 Plot of Normalized growth rate $\gamma/\hat{\omega}_{ci}$ versus $\hat{\omega}_{pi}R_0/c$ for ℓ=2, and (a) η=0.95, (b) η= -0.9.

Fig. 13 Plot of growth rate $\gamma/\hat{\omega}_{ci}$ versus η for ℓ=2 and $\hat{\omega}_{pi}R_0/c$=10.

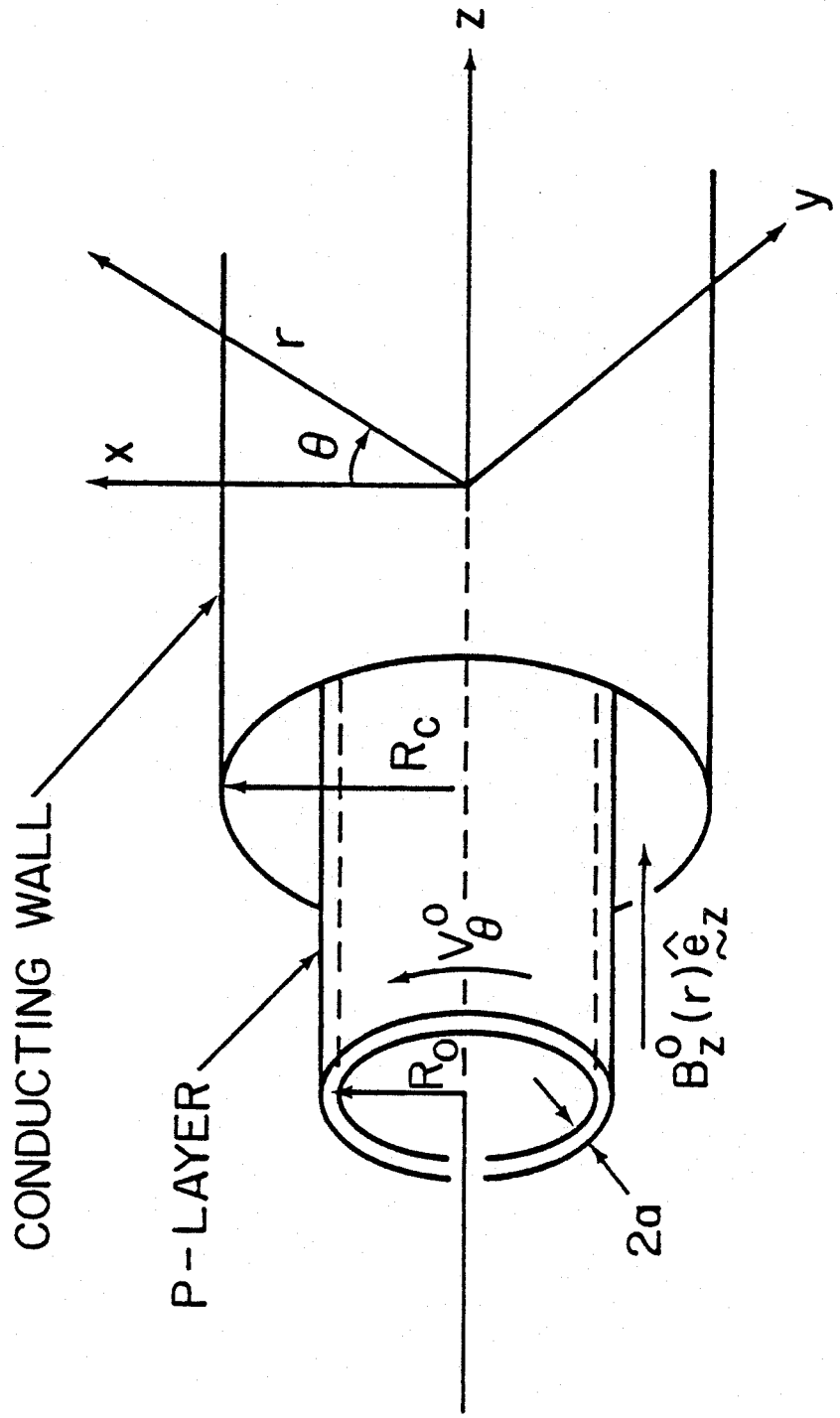

Fig. 1

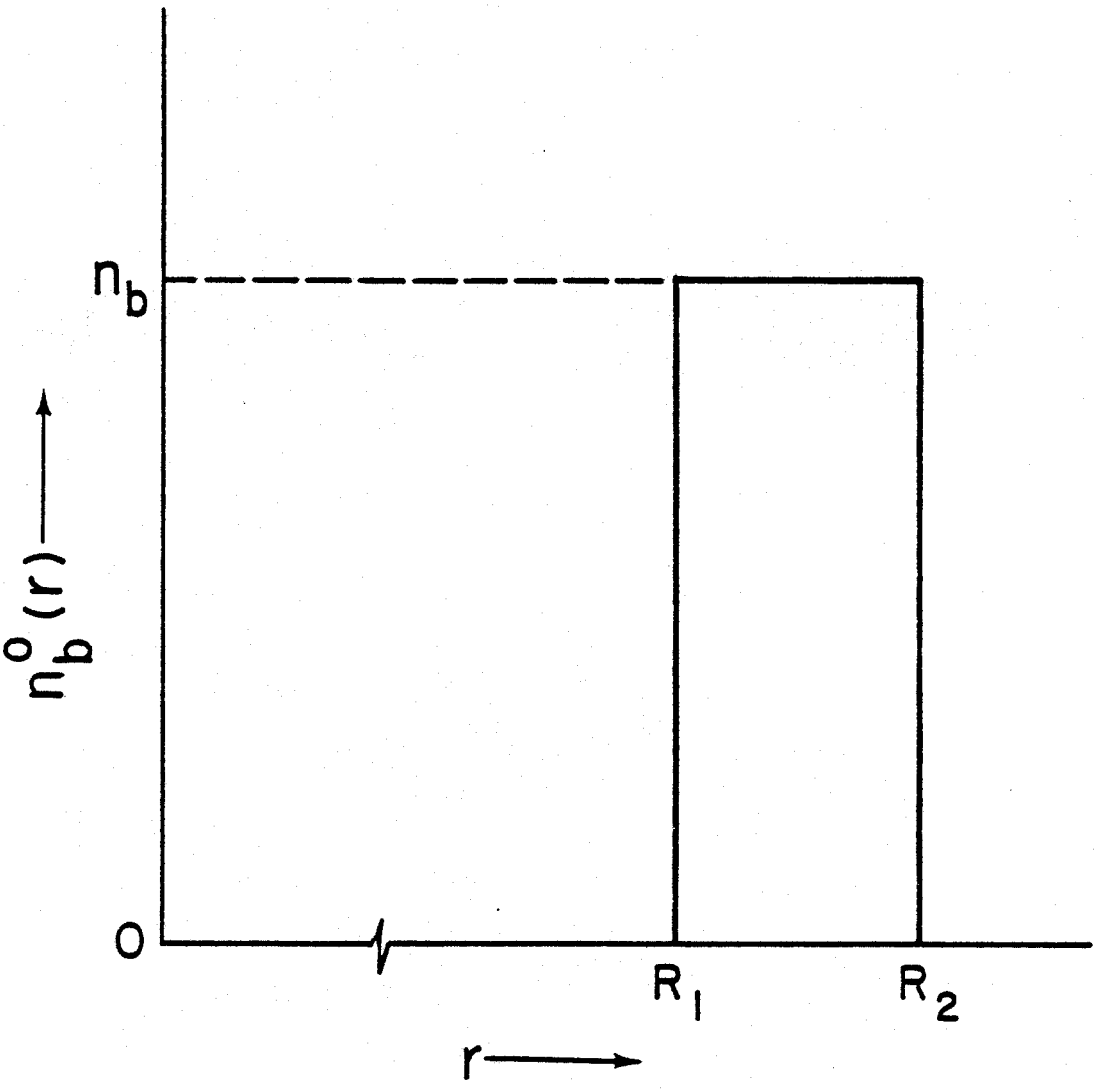

Fig. 2

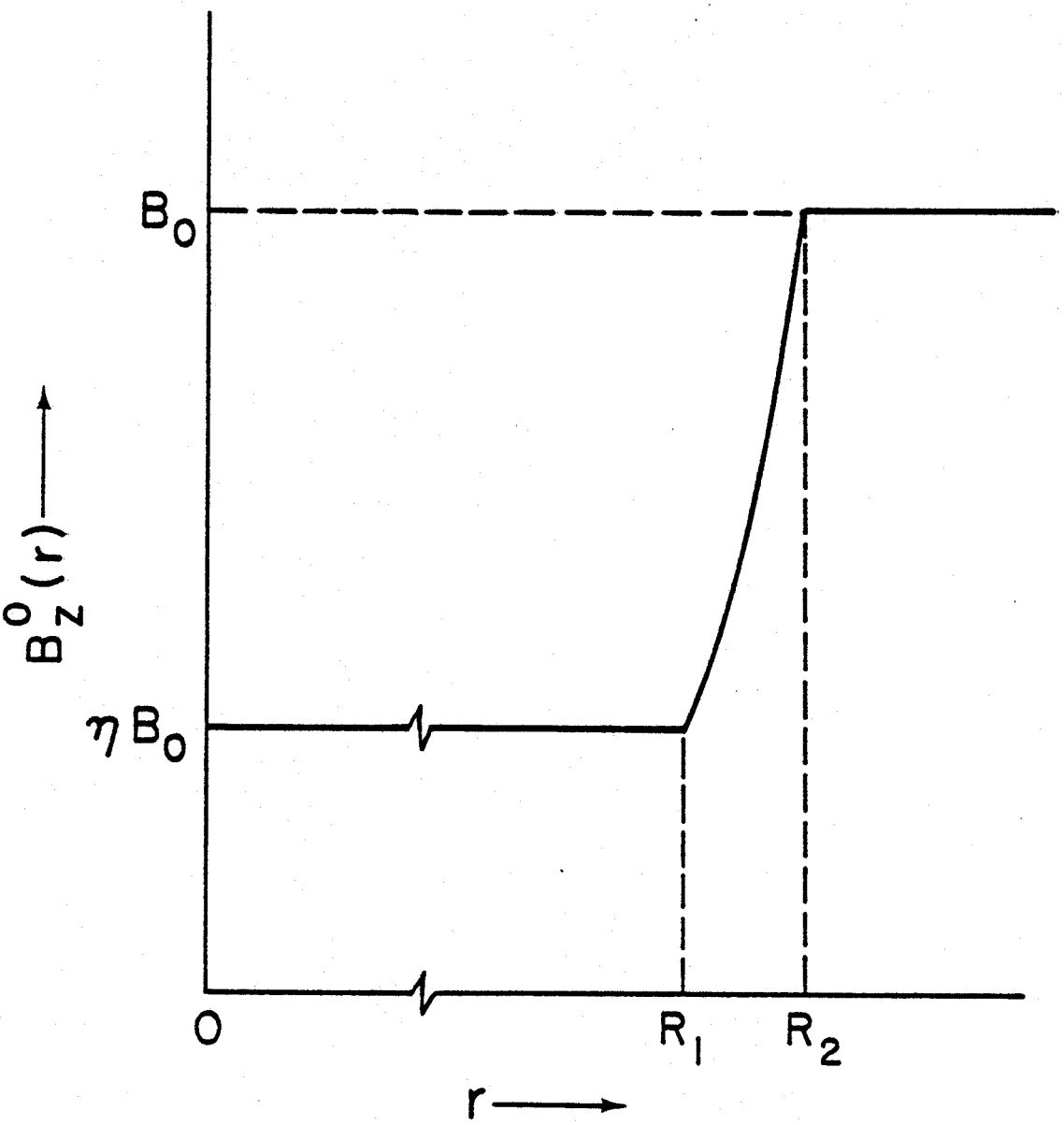

Fig. 3

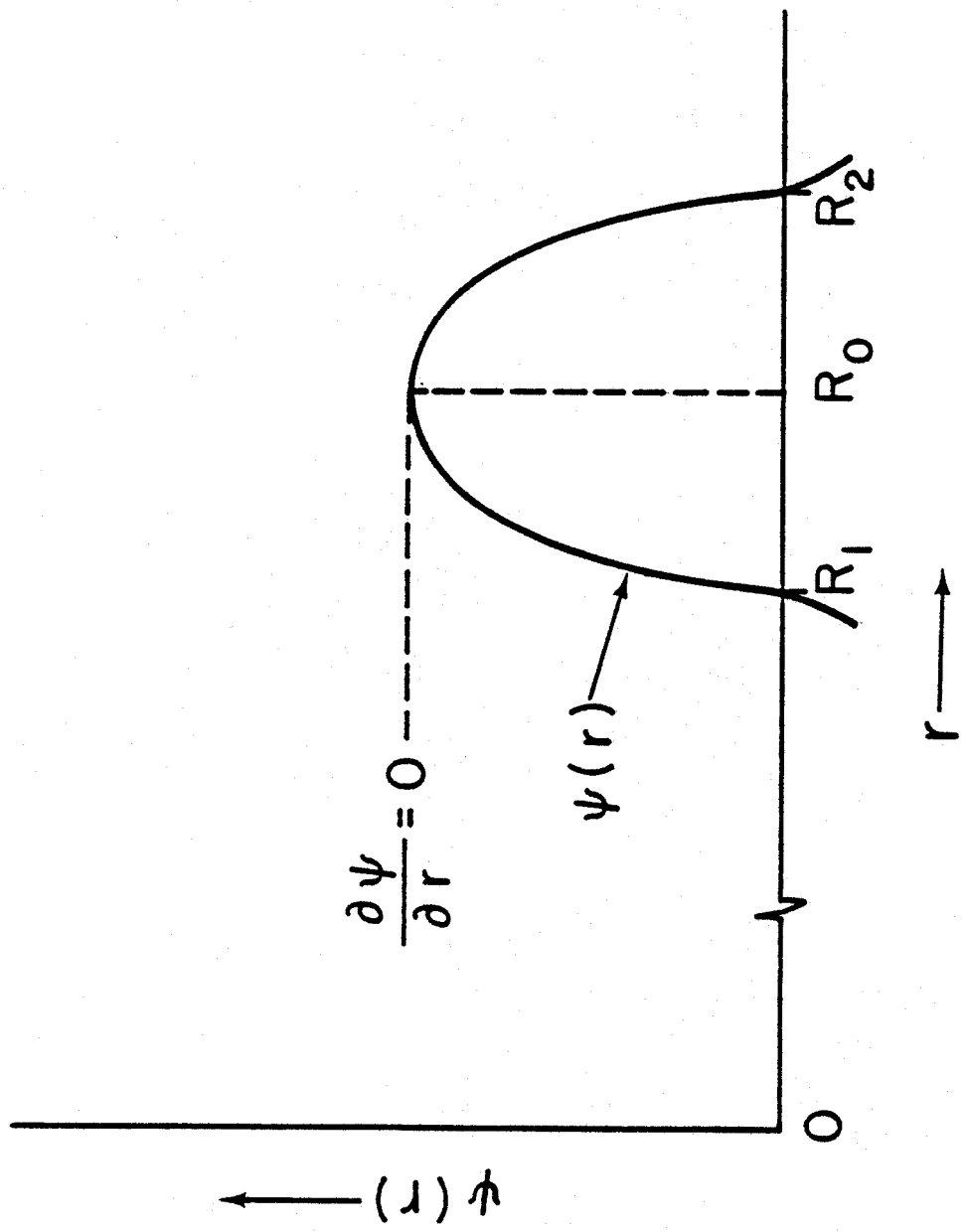

Fig. 4

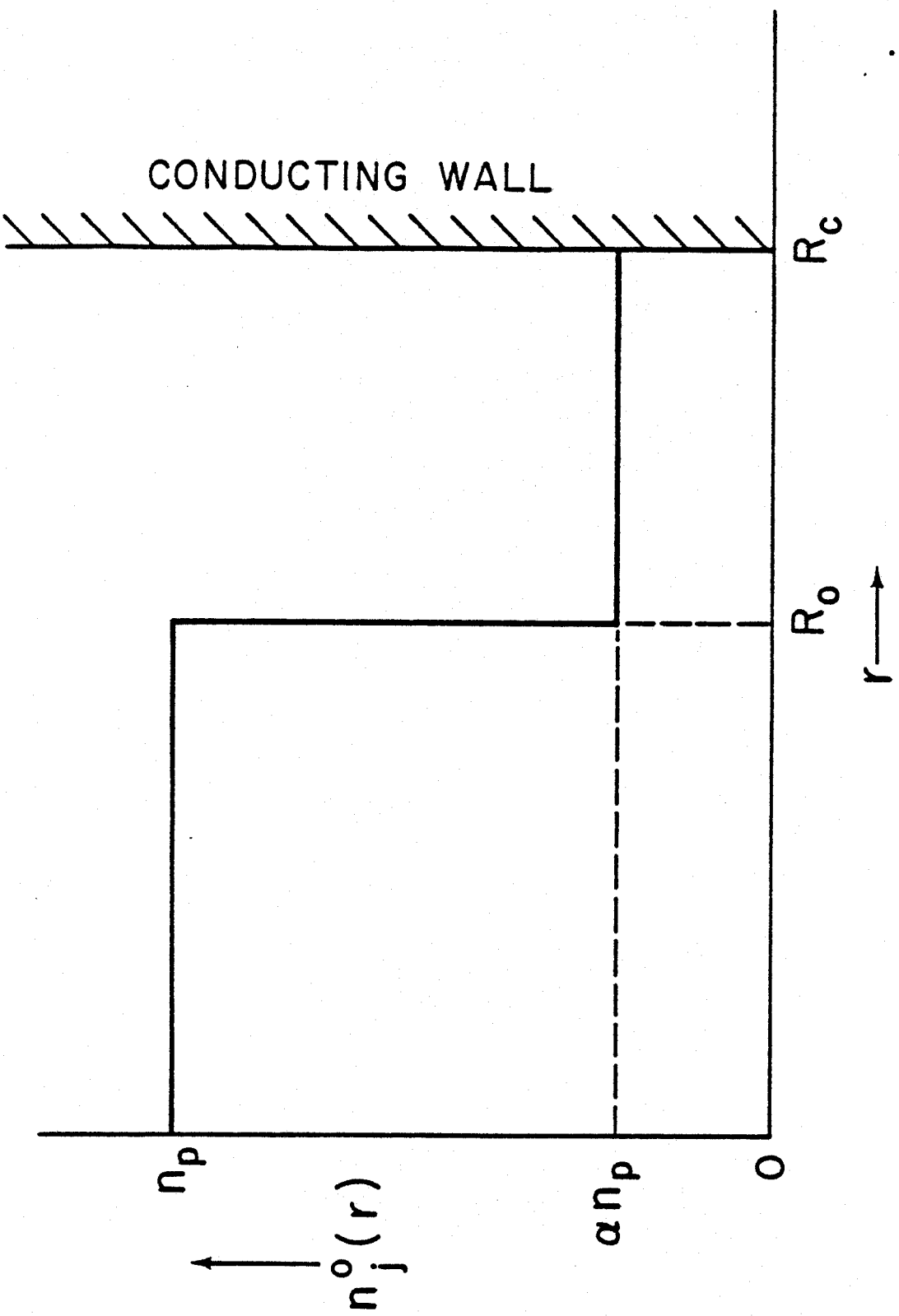

Fig. 5

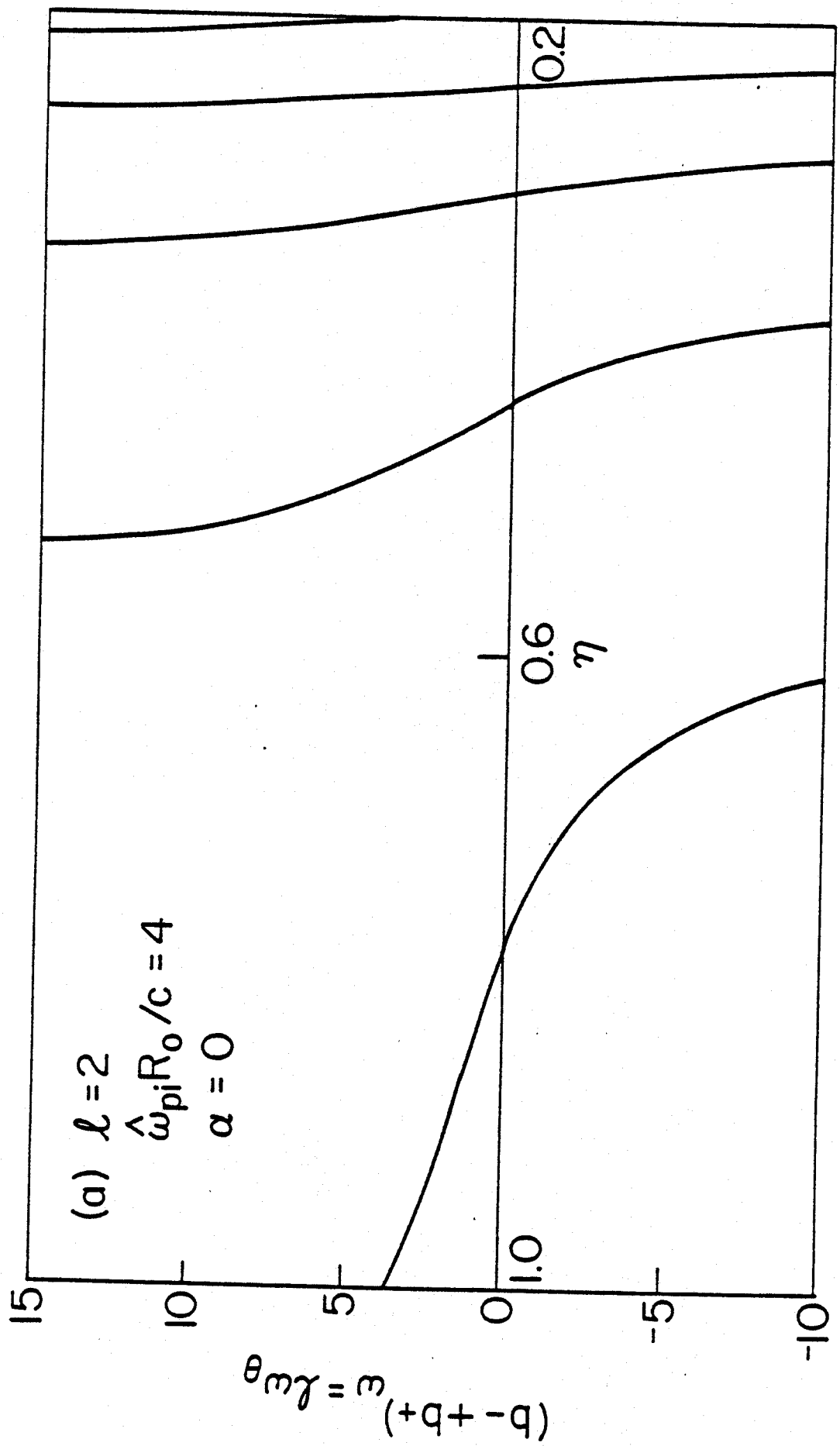

Fig. 6a

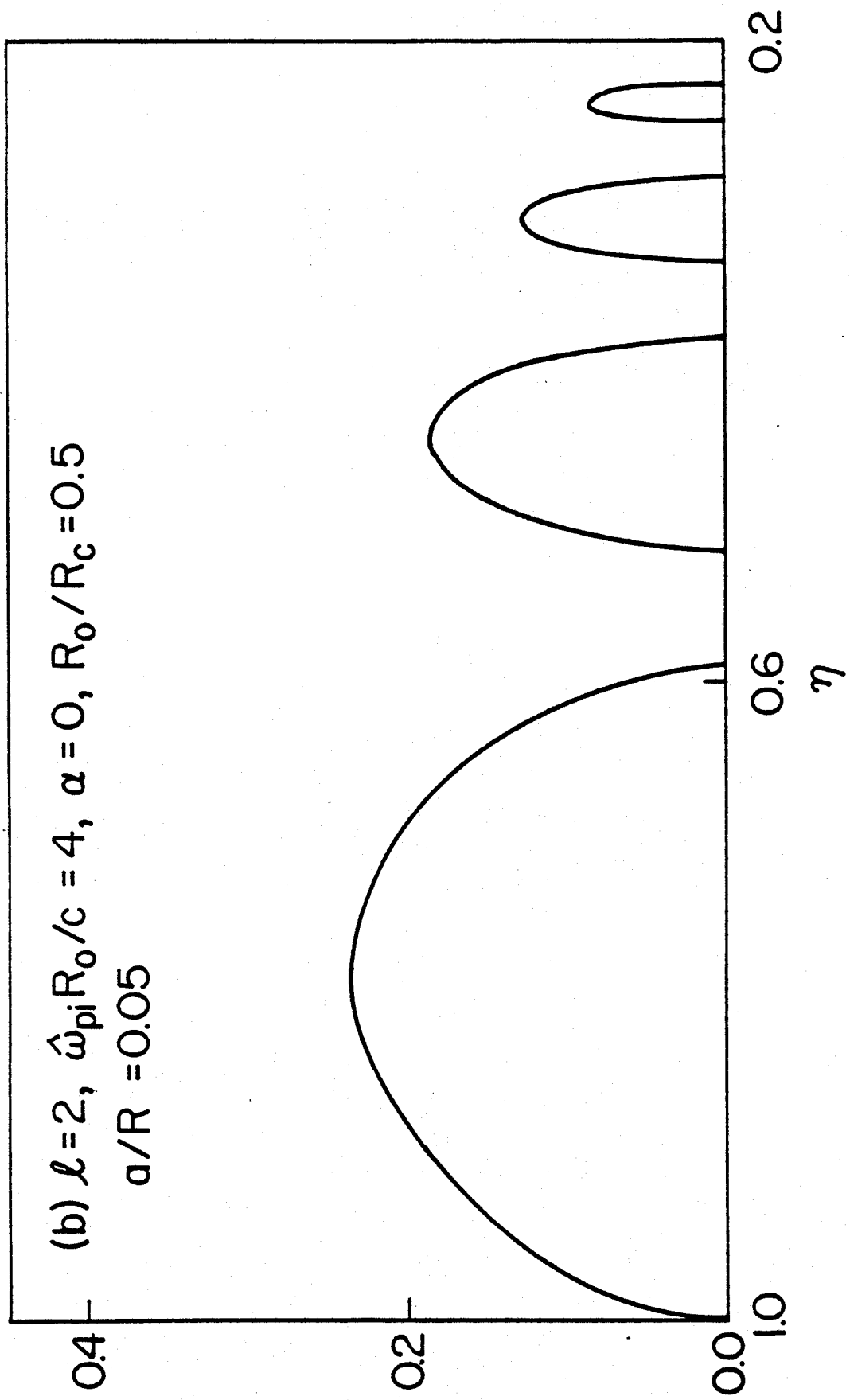
(b) $\ell=2$, $\hat{\omega}_{pi}R_o/c=4$, $\alpha=0$, $R_o/R_c=0.5$
$a/R=0.05$
0.4
0.2
0.0
1.0
0.6
0.2
η
$\frac{\gamma}{\hat{\omega}_{ci}}$

Fig. 6b

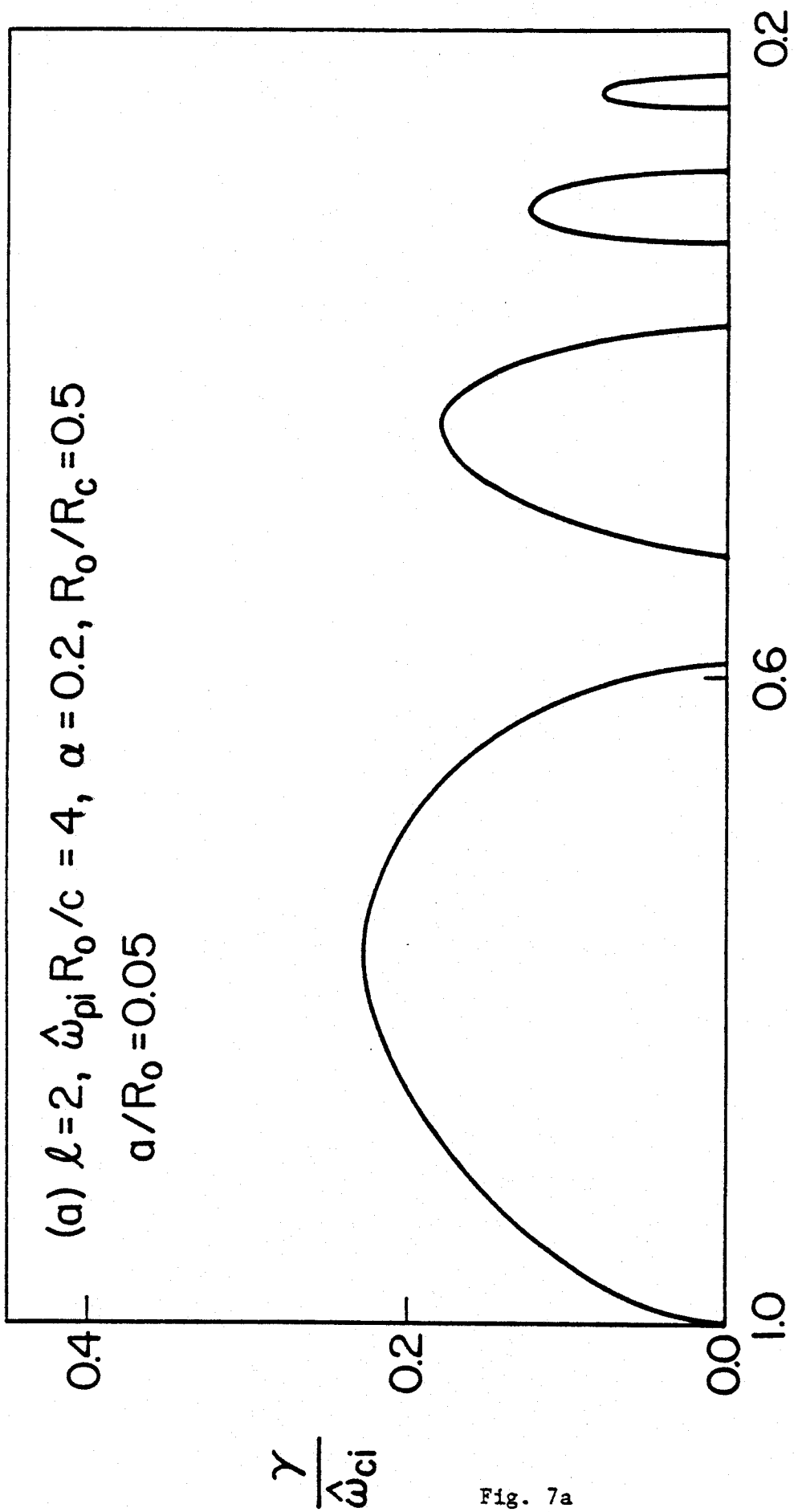
(a) $\ell=2$, $\hat{\omega}_{pi} R_o/c = 4$, $a = 0.2$, $R_o/R_c = 0.5$
$a/R_o = 0.05$
$\frac{\gamma}{\hat{\omega}_{ci}}$
0.4
0.2
0.0
1.0
0.6
0.2
η

Fig. 7a

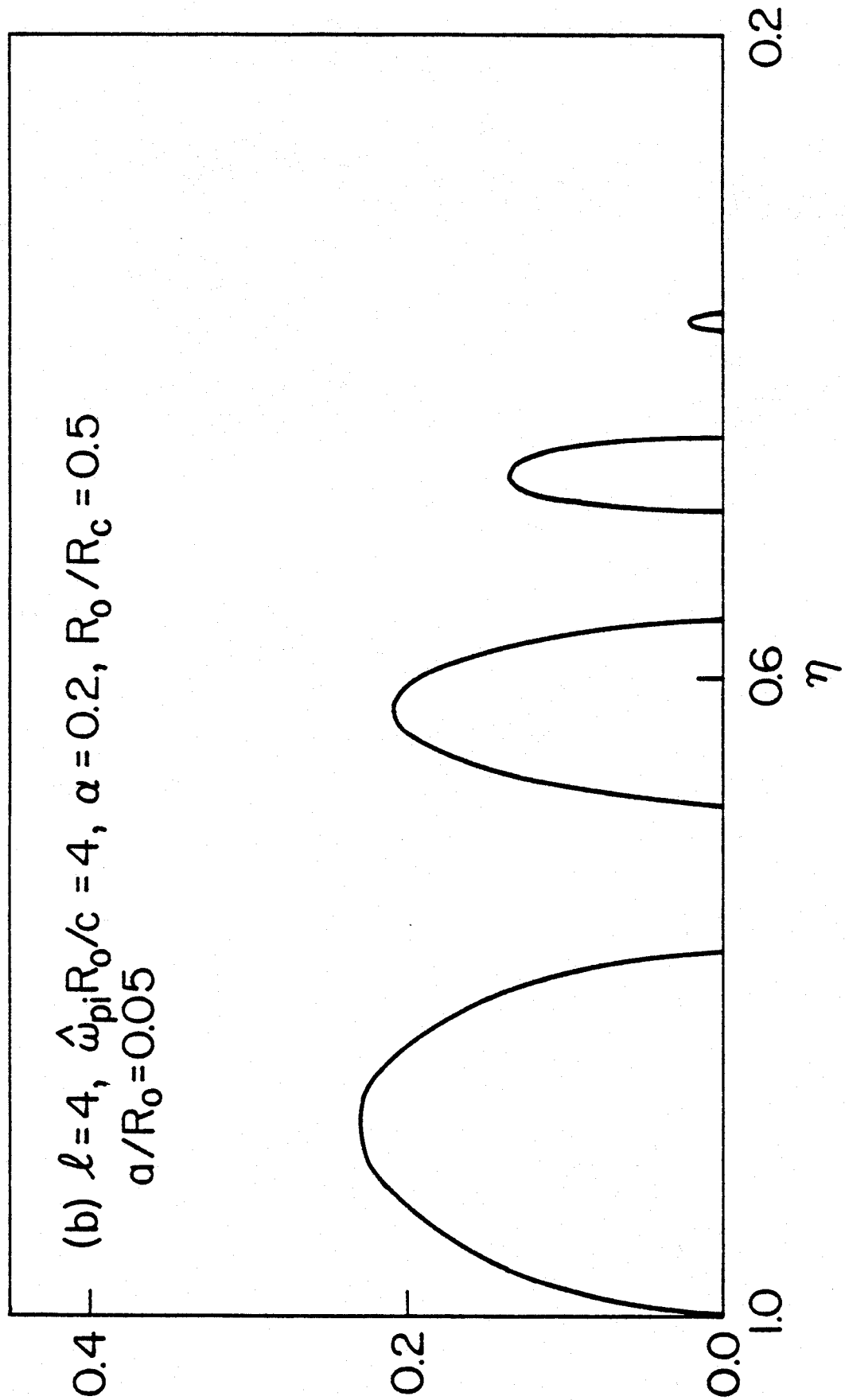
(b) $\ell=4$, $\hat{\omega}_{pi}R_0/c=4$, $a=0.2$, $R_0/R_c=0.5$
$a/R_0=0.05$
0.4
0.2
0.0
1.0
0.6
0.2
η
$\frac{\gamma}{\hat{\omega}_{ci}}$

Fig. 7b

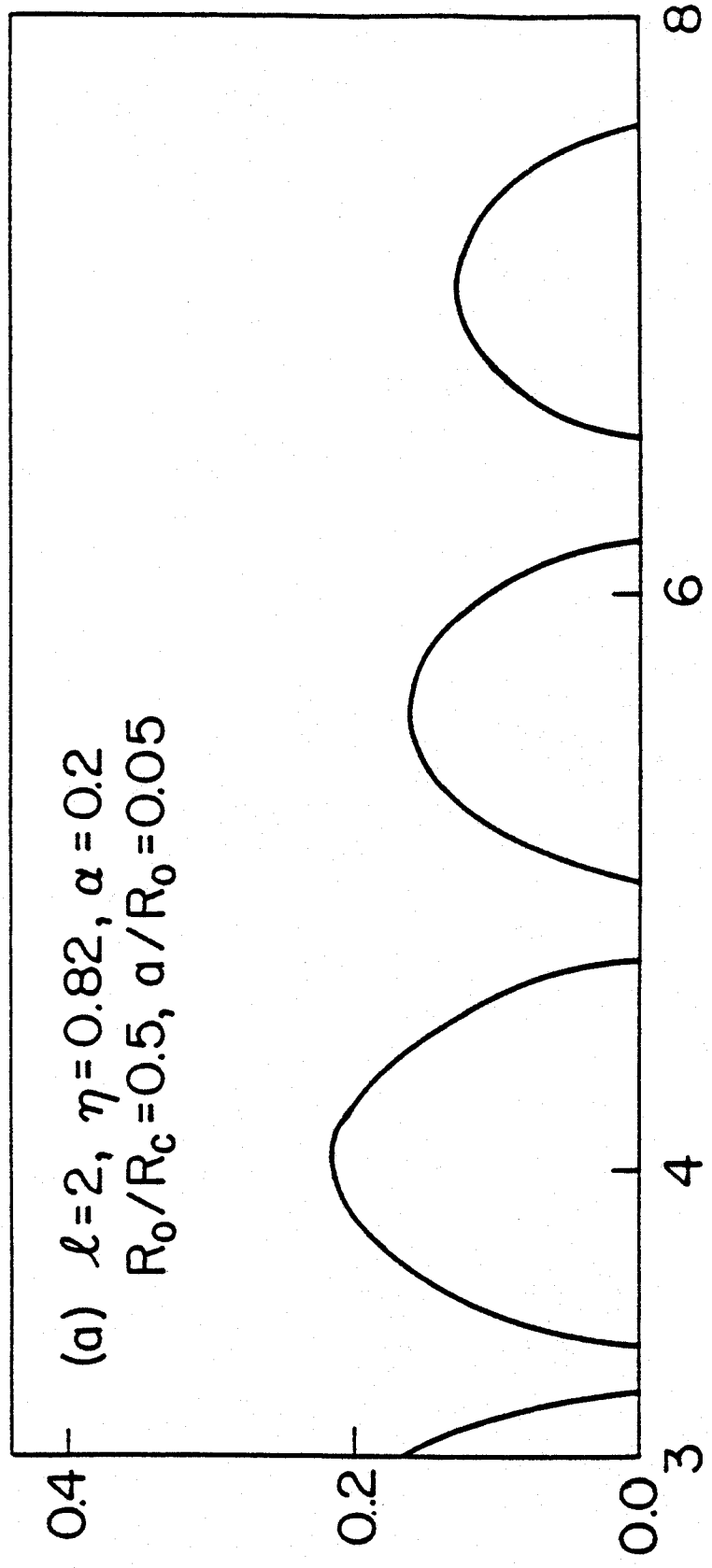

Fig. 8a

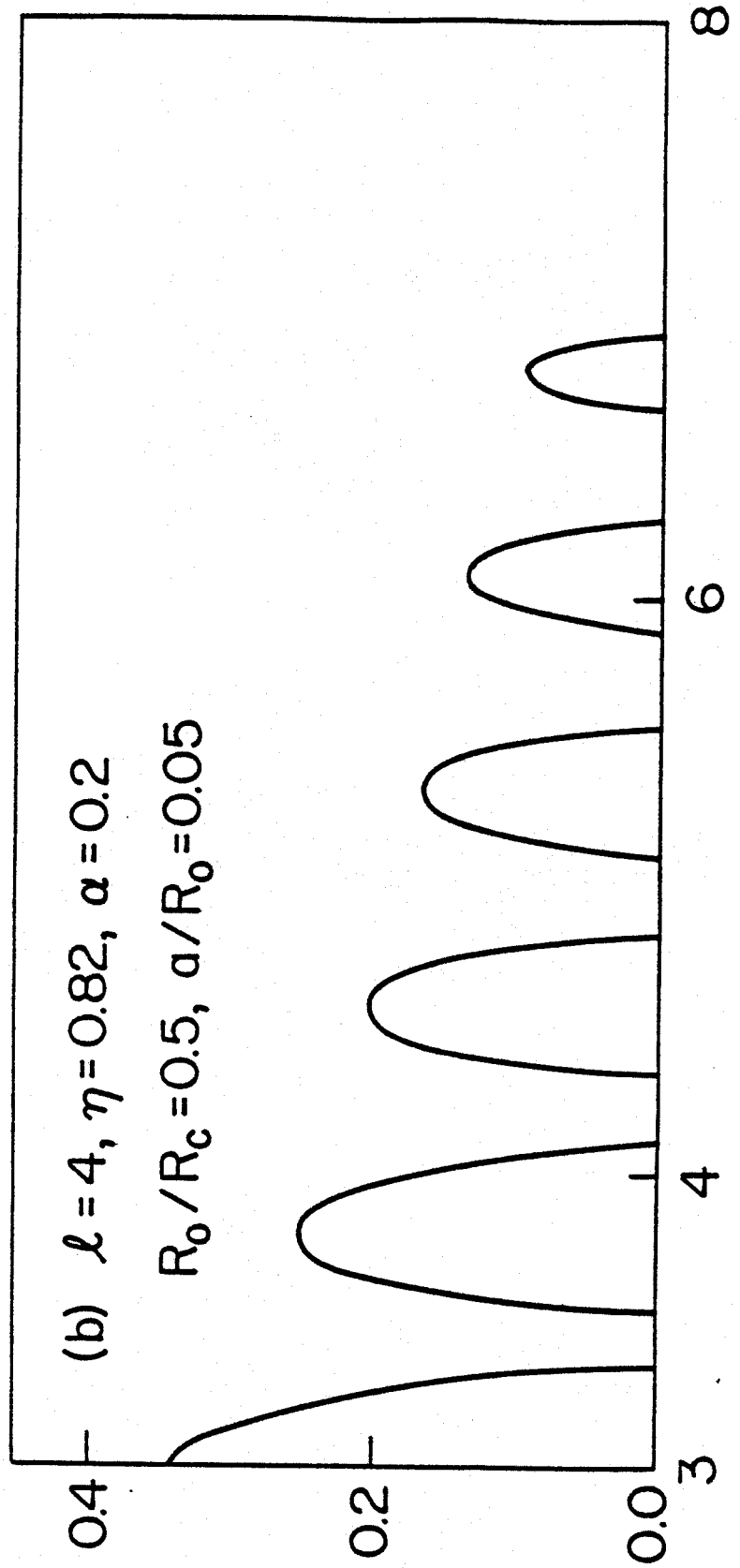
(b) $\ell = 4$, $\eta = 0.82$, $\alpha = 0.2$
$R_o/R_c = 0.5$, $a/R_o = 0.05$
0.4
0.2
0.0
3
4
6
8
$\frac{\gamma}{\hat{\omega}_{ci}}$
$\hat{\omega}_{pi} R_o/c$

Fig. 8b

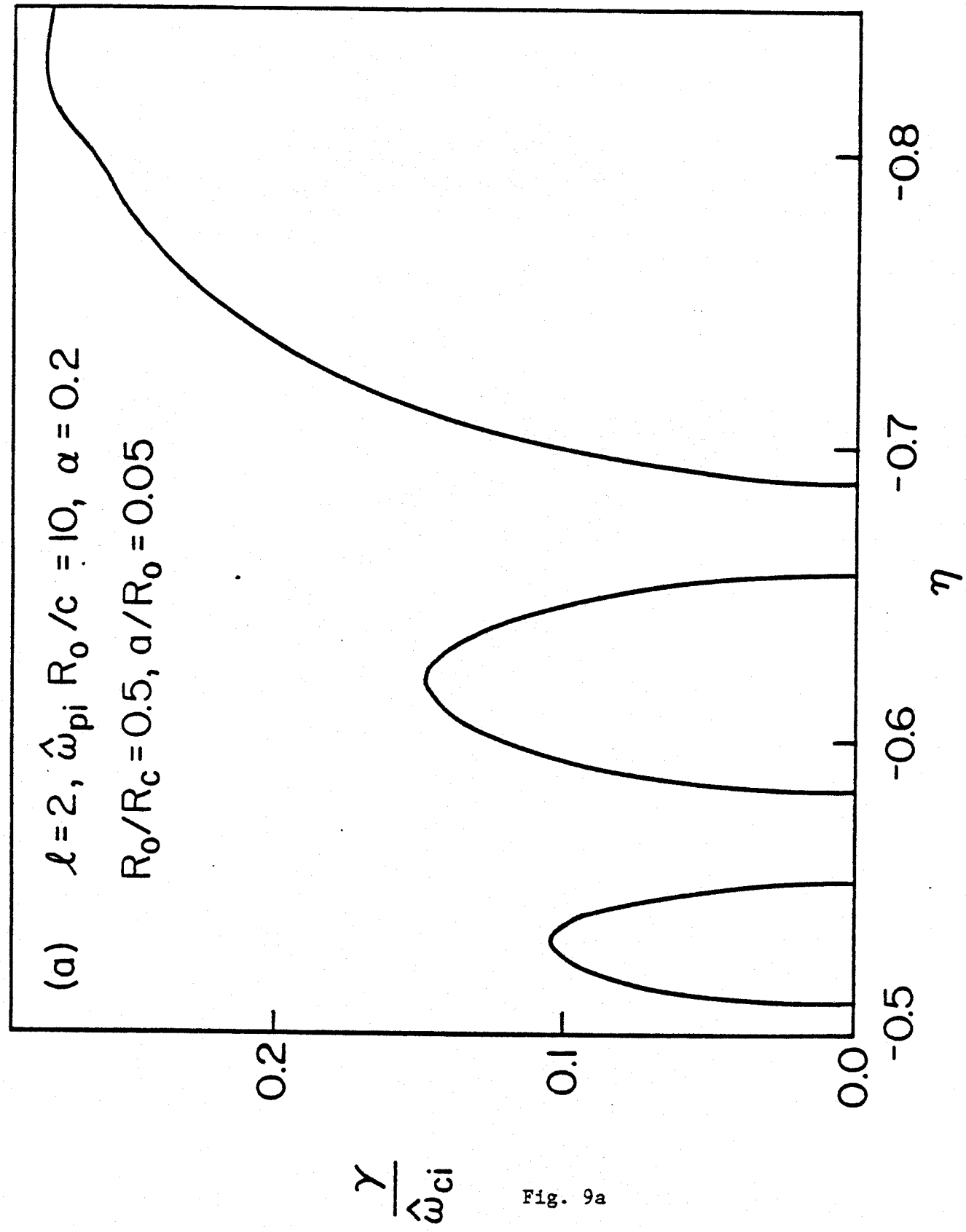
(a) $\ell = 2$, $\hat{\omega}_{pi} R_o/c = 10$, $\alpha = 0.2$
$R_o/R_c = 0.5$, $a/R_o = 0.05$
0.2
0.1
0.0
-0.5
-0.6
-0.7
-0.8
η
$\frac{\gamma}{\hat{\omega}_{ci}}$

Fig. 9a

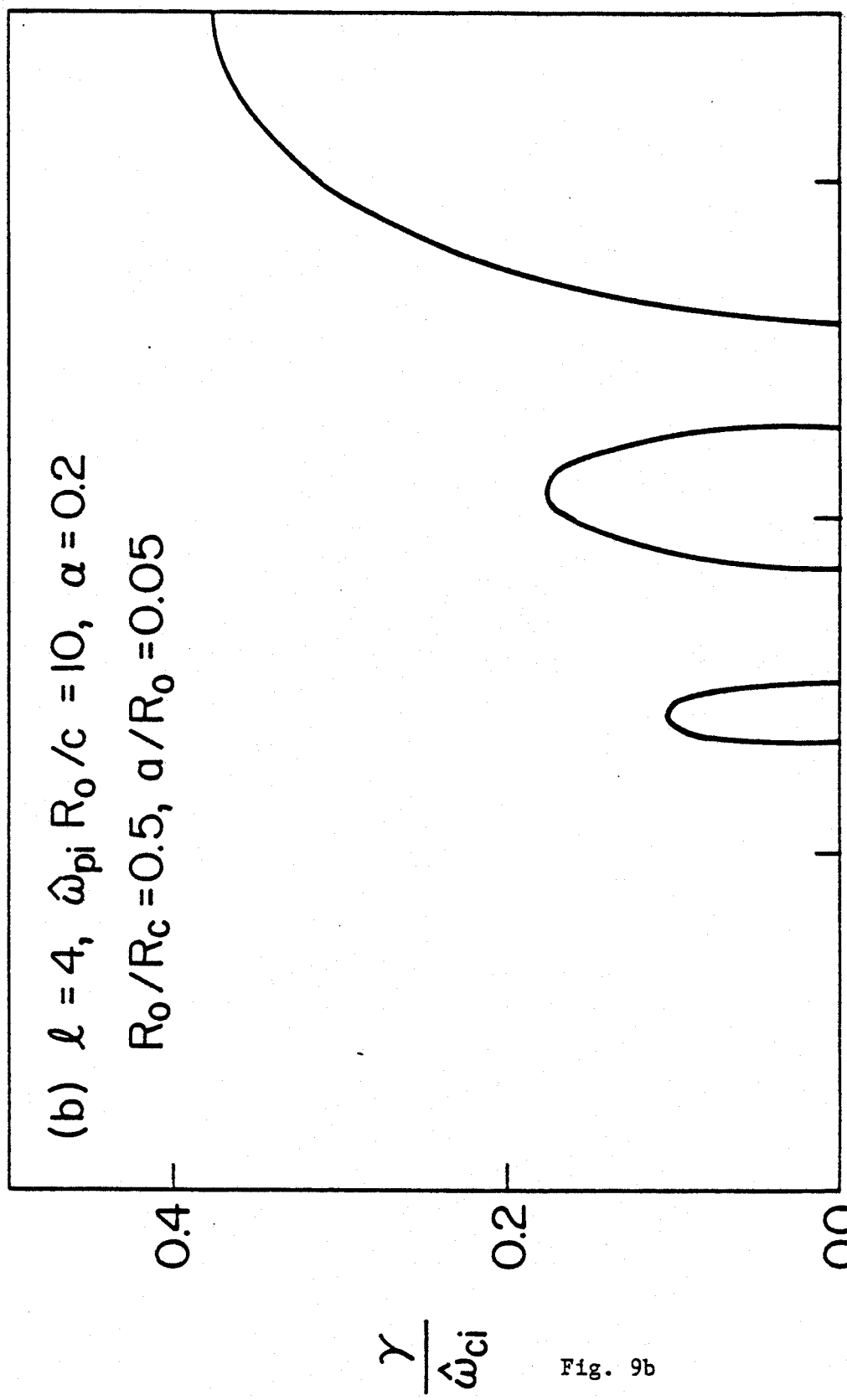
(b) $\ell = 4$, $\hat{\omega}_{pi} R_o/c = 10$, $a = 0.2$
$R_o/R_c = 0.5$, $a/R_o = 0.05$
0.4
0.2
0.0
-0.5
-0.6
-0.7
-0.8
η
$\frac{\gamma}{\hat{\omega}_{ci}}$

Fig. 9b

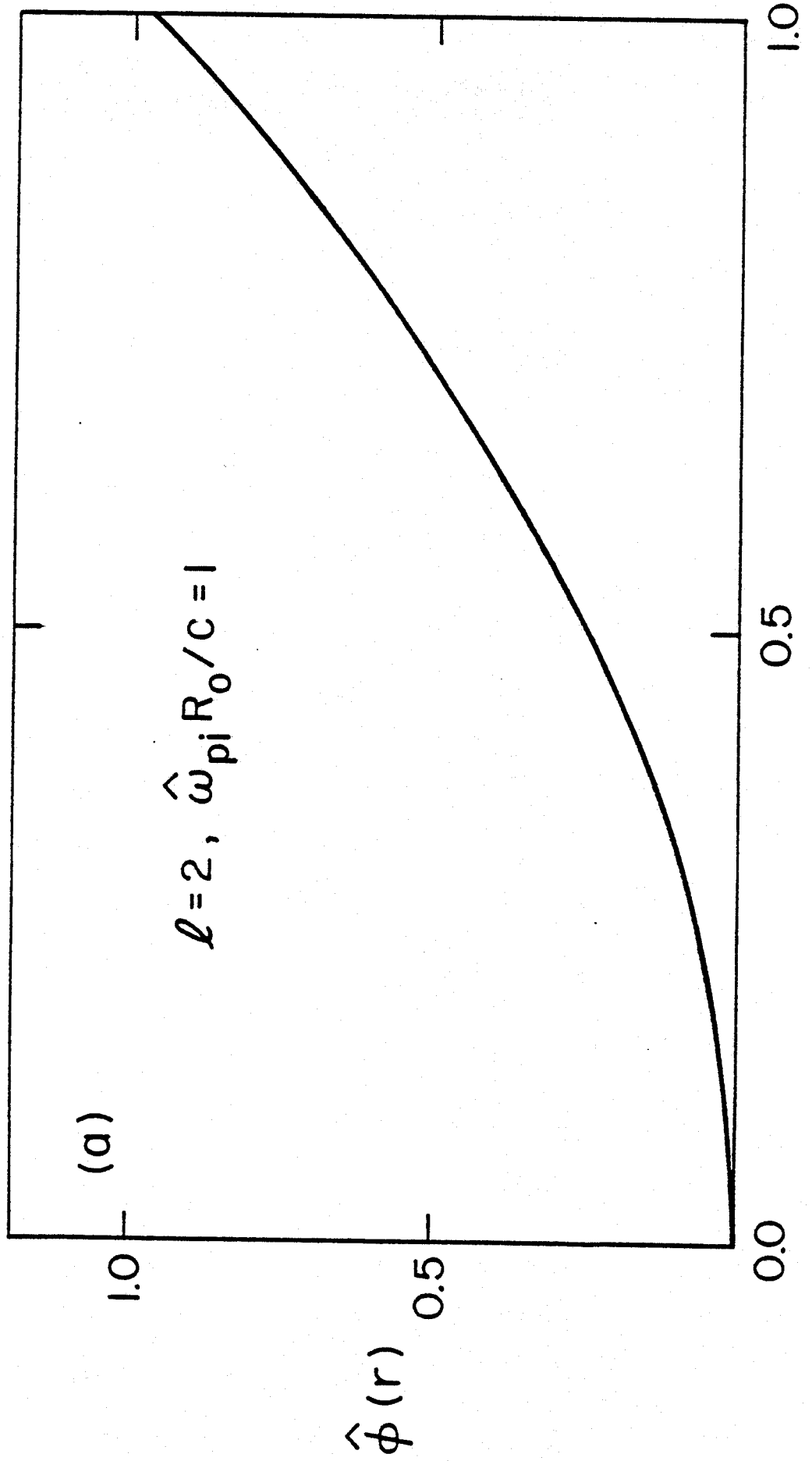

Fig. 10a

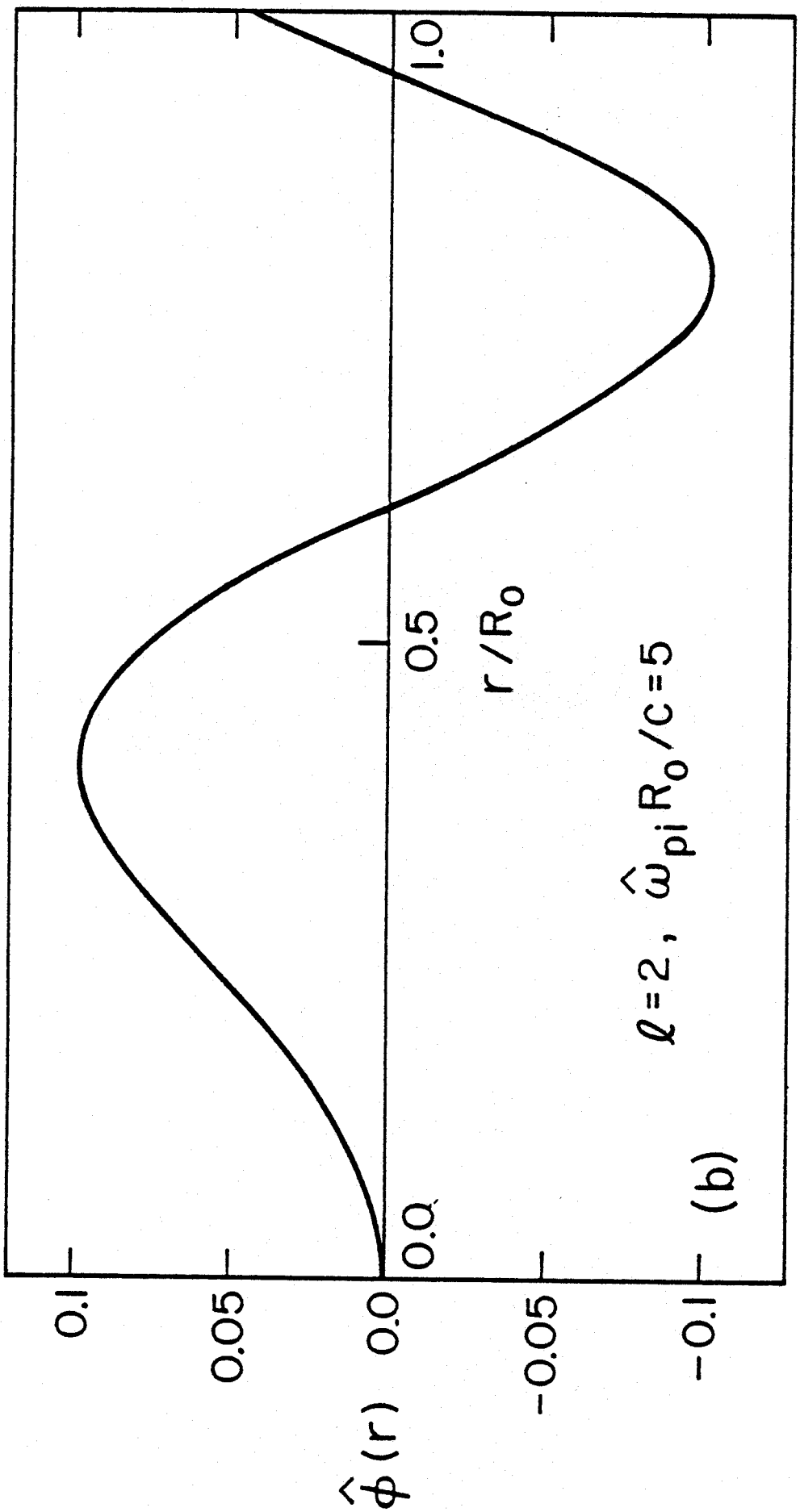

Fig. 10b

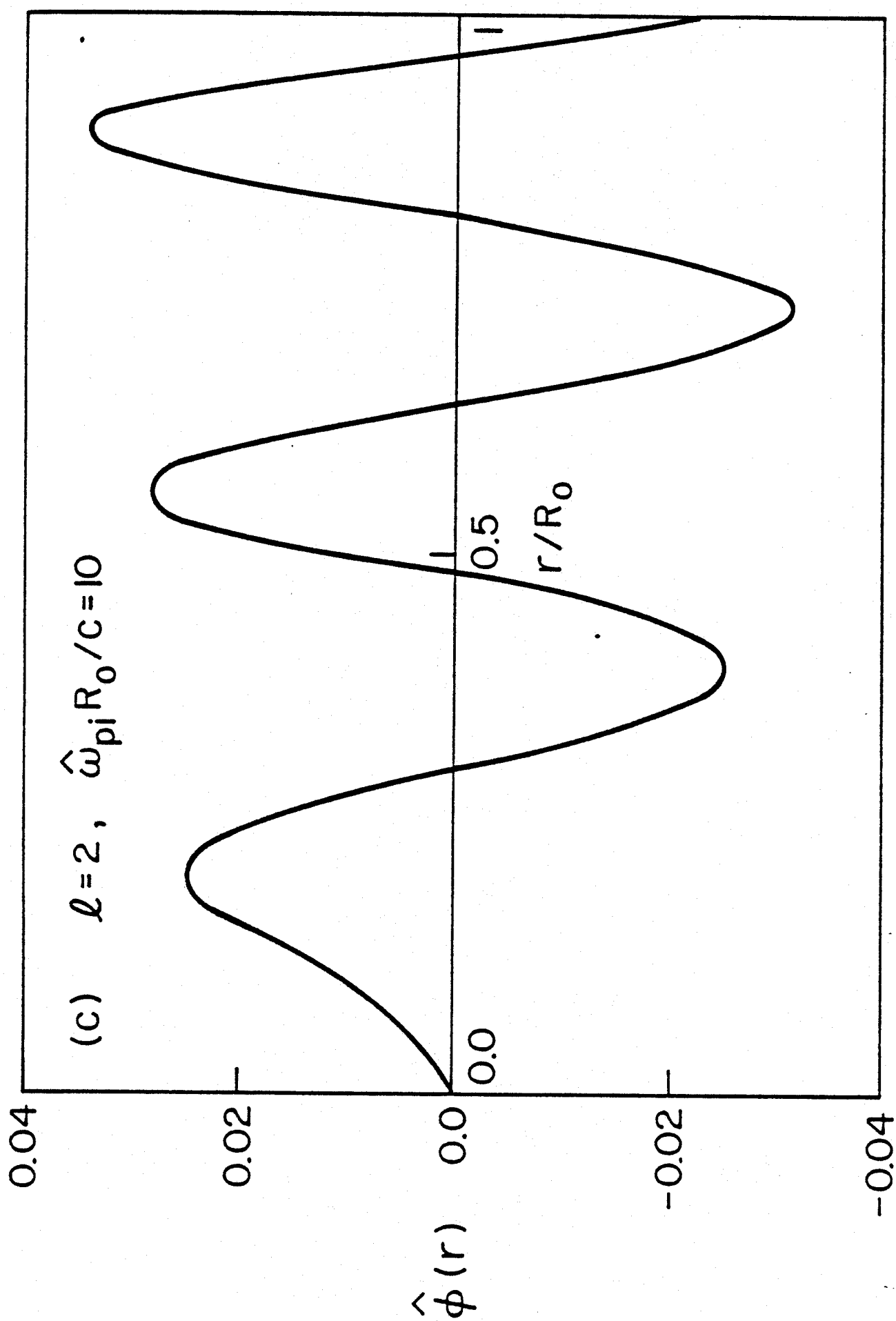
(c) $\ell=2$, $\hat{\omega}_{pi}R_o/c=10$
0.04
0.02
0.0
-0.02
-0.04
$\hat{\phi}(r)$
0.0
0.5
1
r/R_o

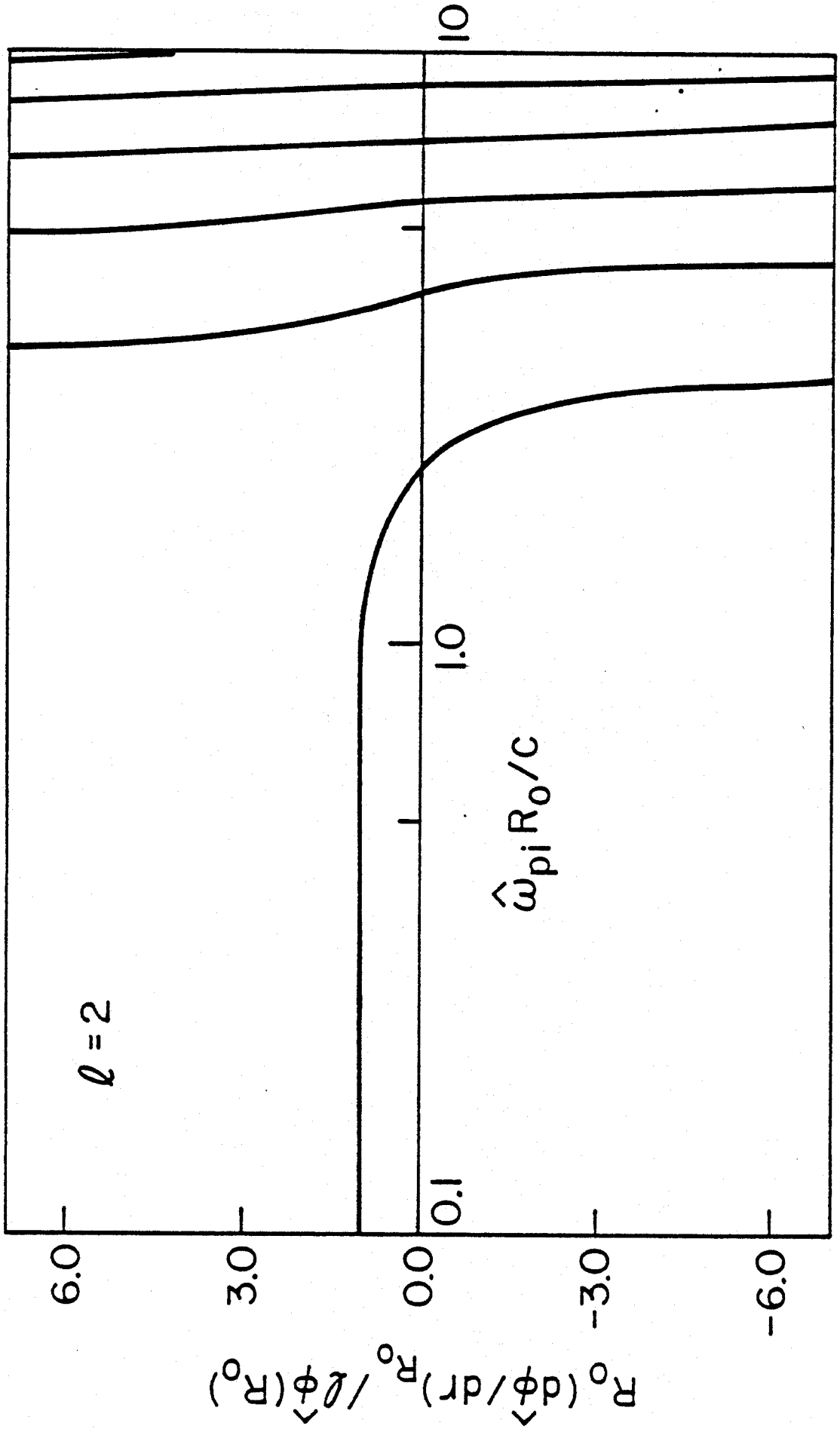
10
1.0
0.1
$\hat{\omega}_{pi} R_o/c$
$\ell = 2$
6.0
3.0
0.0
-3.0
-6.0
$R_o (d\hat{\phi}/dr)_{R_o} / \ell \hat{\phi}(R_o)$

Fig. 11

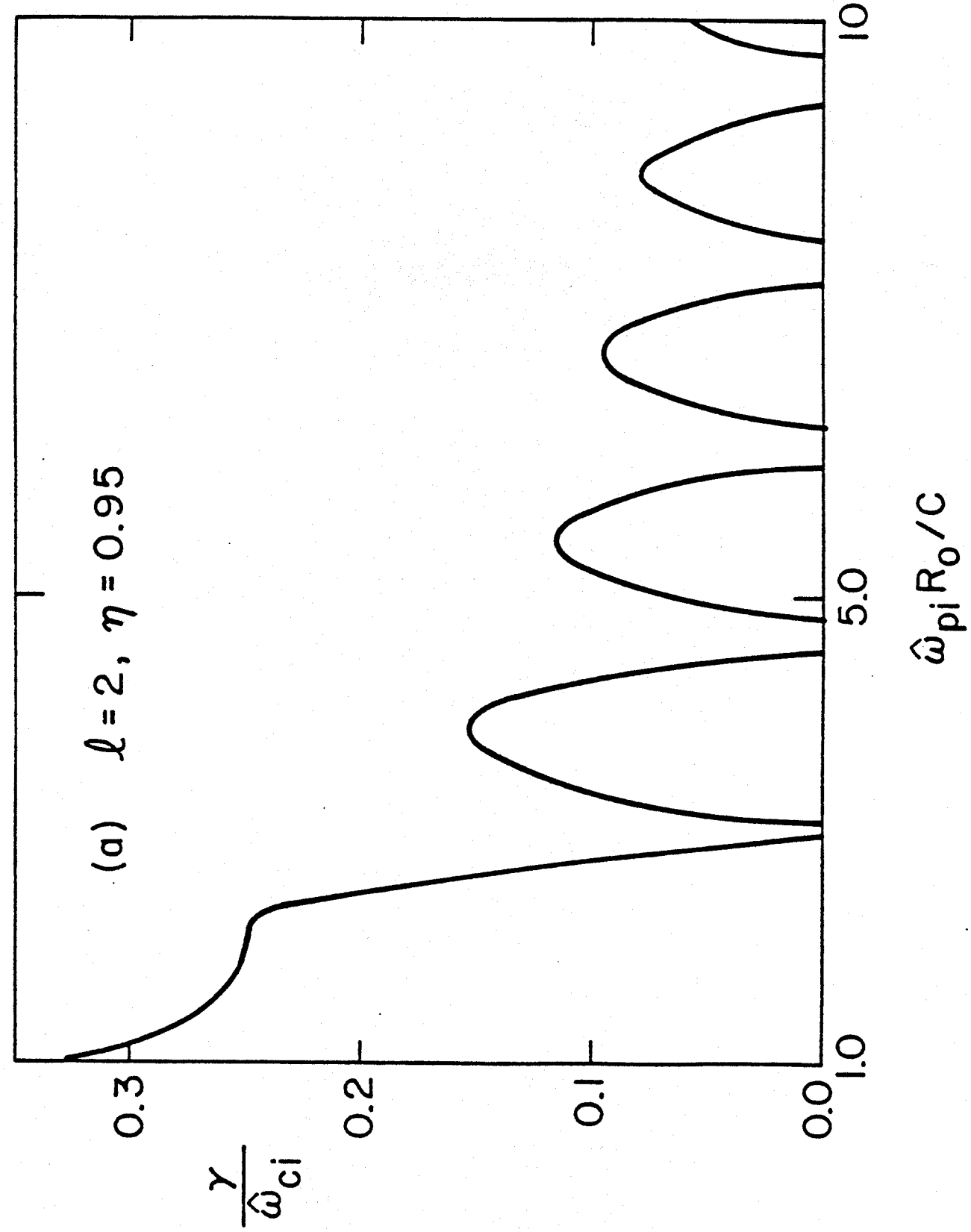
(a) $\ell = 2$, $\eta = 0.95$
$\frac{\gamma}{\hat{\omega}_{ci}}$
0.3
0.2
0.1
0.0
1.0
5.0
10
$\hat{\omega}_{pi} R_o / C$

Fig. 12a

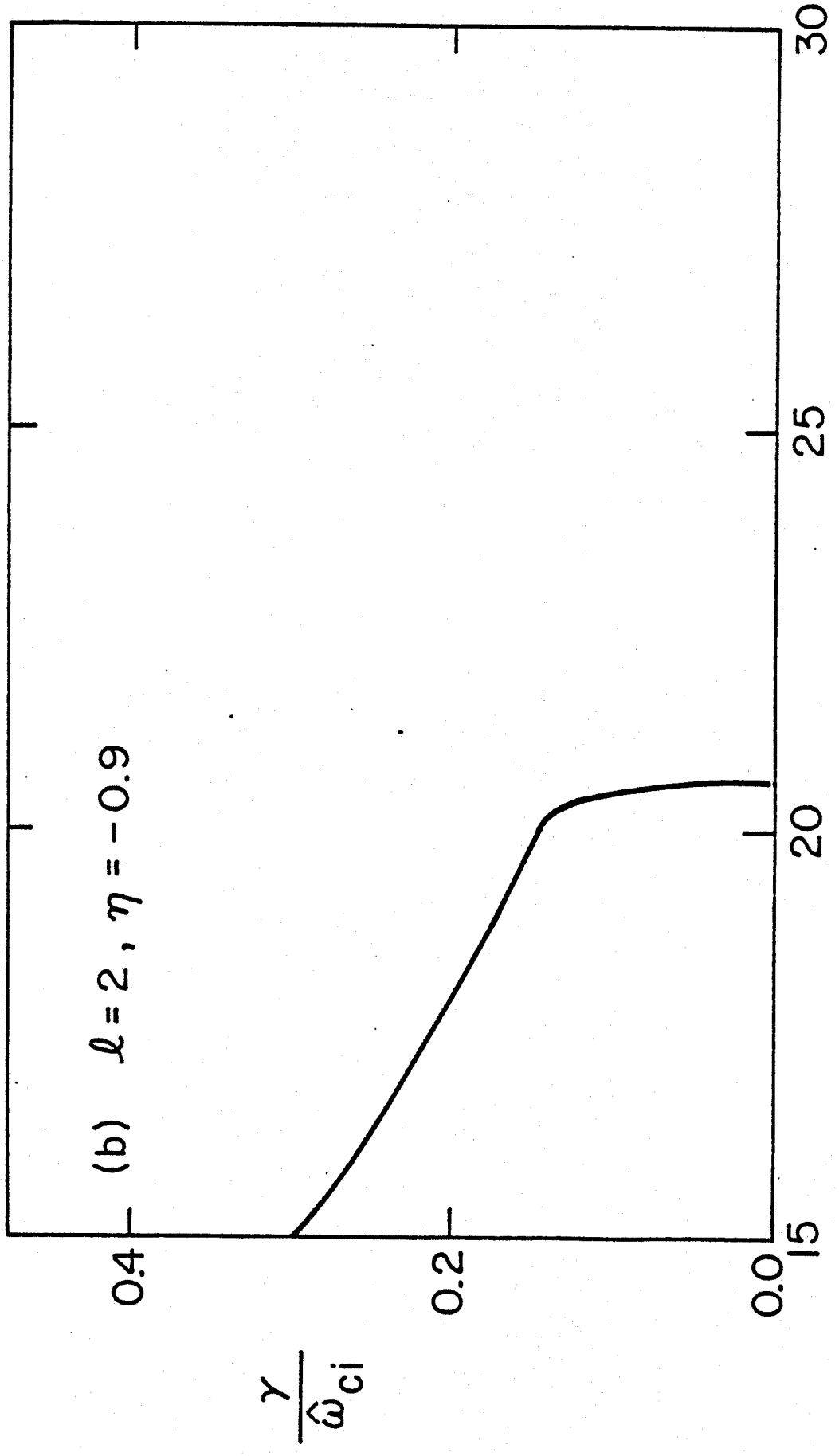
(b) $\ell = 2, \eta = -0.9$
$\frac{\gamma}{\hat{\omega}_{ci}}$
0.4
0.2
0.0
15
20
25
30
$\hat{\omega}_{pi} R_o / C$

Fig. 12b

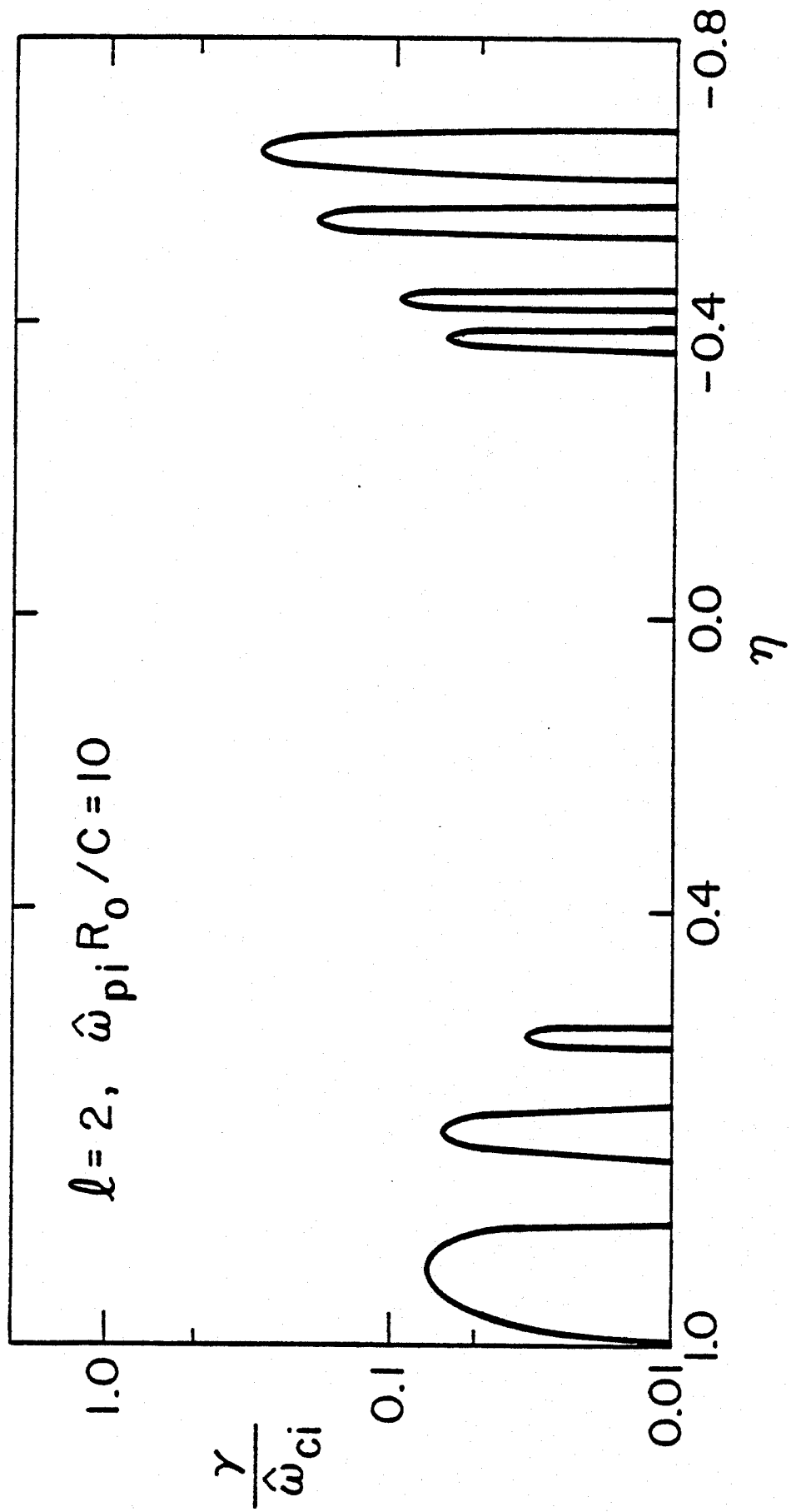
$\ell = 2,\ \hat{\omega}_{pi} R_0 / C = 10$
$\frac{\gamma}{\hat{\omega}_{ci}}$
1.0
0.1
0.01
-0.8
-0.4
0.0
0.4
1.0
η

Fig. 13